Synthesis and Structures of Main Group Cage Compounds Containing Boron, Silicon, and Phosphorus Atoms

Danan Dou,[†] Bernhard Kaufmann,[‡] Eileen N. Duesler,[†] Tuqiang Chen,[†] Robert T. Paine,[*,†] and H. Nöth[*,‡]

Department of Chemistry, University of New Mexico, Albuquerque, New Mexico 87131, and Institüt für Anorganische Chemie, Universität München, 8000-München 2, FRG

Received December 21, 1992

The reactions of lithium salts $[(i\text{-}Pr_2N)\overline{BP(H)B(N\text{-}i\text{-}Pr_2)P}Li\cdot DME]$ and $[tmp\overline{BP(H)B(tmp)P}Li\cdot DME]$ (tmp = 2,2,6,6-tetramethylpiperidino) with organylhalosilanes have been surveyed, and silyl-substituted diphosphadiboretanes of the general types $R_2N\overline{BP(H)B(NR_2)P}SiR'_3$ (R_2N = i-Pr_2N, tmp; SiR'_3 = $SiMe_2Ph$) and $R_2N\overline{BP(H)B(NR_2)P}SiR'_2$-Cl ($R_2N$ = i-Pr_2N, tmp; SiR'_2Cl = $SiMe_2Cl$, $SiPh_2Cl$, $Me_2SiSiMe_2(Cl)$) have been isolated and characterized. Dehydrohalogenation of the latter class of compounds with *t*-BuLi provides an efficient route to new bicyclic cage compounds $P_2(BNR_2)_2(SiR_2)$ and $P_2(BNR_2)_2[Si(R)_2SiR_2]$. Alternatively, the cage compounds $P_2(tmpB)_2SiR_2$ (R_2 = Ph_2, Me_2, Ph(Me)) have been obtained by combination of the dipotassium salt $K_2[tmp\overline{BPB(tmp)P}]$ and R_2SiCl_2. The coordination chemistry of the ligands has been surveyed, and a series of $Fe(CO)_4\cdot L$ complexes has been isolated. Attempts to form bimetallic complexes were unsuccessful. The structures of several compounds have been determined by single-crystal X-ray diffraction techniques with Mo Kα radiation (λ = 0.710 73 Å): $P_2(i\text{-}Pr_2NB)_2(SiPh_2)$, $C_{24}H_{38}B_2N_2P_2Si$, crystallized in the triclinic space group $P\bar{1}$ with a = 11.116(2) Å, b = 11.436(2) Å, c = 14.225(2) Å, α = 67.28(1)°, β = 67.66(1)°, γ = 61.10(1)°, and z = 2; $P_2(tmpB)_2SiPh_2$, $C_{30}H_{46}B_2N_2P_2Si$, crystallized in the orthorhombic space group *Pbca* with a = 14.445(9) Å, b = 19.18(2) Å, c = 23.25(2) Å, and Z = 8; $P_2(tmpB)_2(SiMe_2)_2$, $C_{22}H_{48}B_2N_2P_2Si_2$, crystallized in the orthorhombic space group *Pnma* with a = 11.375(2) Å, b = 14.977(2) Å, c = 16.939(4) Å, and Z = 4; $i\text{-}Pr_2N\overline{BP(H)B(N\text{-}i\text{-}Pr_2)P}Si(Me)_2Si(Me)_2\overline{PB(N\text{-}i\text{-}Pr_2)P(H)B}N\text{-}i\text{-}Pr_2$, $C_{14}H_{35}B_2N_2P_2Si$, crystallized in the monoclinic space group $P2_1/n$ with a = 10.994(2) Å, b = 15.320(2) Å, c = 13.389(3) Å, β = 101.93(1)°, and Z = 4; $P_2(i\text{-}Pr_2NB)_2(SiMe_2)_2$, $C_{16}H_{40}B_2N_2P_2Si_2$, crystallized in the orthorhombic space group $P2_12_12_1$ with a = 12.366(2) Å, b = 13.377(2) Å, c = 15.077(4) Å, and Z = 4; $P_2(i\text{-}Pr_2NB)_2(SiPh_2)\cdot Fe(CO)_4$, $C_{28}H_{38}B_2N_2O_4P_2SiFe$, crystallized in the monoclinic space group $P2_1/n$ with a = 14.403(3) Å, b = 15.550(4) Å, c = 15.632(3) Å, β = 102.07(1)°, and Z = 4; $P_2(tmpB)_2(SiMe_2)\cdot Fe(CO)_4$ crystallized in the monoclinic space group $P2_1/c$ with a = 11.132(2) Å, b = 32.531(9) Å, c = 17.504(4) Å, β = 92.19(2)°, and Z = 8. The structural features of these cage compounds are compared with data from cages of the type $P_2(BNR_2)_3$.

Introduction

From a structural standpoint, many closed and open framework main group element cage and cluster compounds can be visualized as ordered collections of edge-sharing, small-ring (3–6 membered) fragments. It is therefore logical to consider small main group element rings as synthetic building blocks for the systematic assembly of new cage and cluster species. Unfortunately, in the past, most main group element rings have been prepared with sterically bulky or chemically inert substituent groups that assist efforts to isolate the compounds but leave them relatively useless for subsequent applications in substituent group elimination–ring coupling chemistry.

In a few instances, small-ring compounds with labile substituents have been prepared, and more complex cage structures have been derived from them. For example, in 1959, Parshall and Lindsey[1] reported a series of metathesis reactions between lithium phosphides, $LiPH_2$, Li_2PH, and Li_3P, and chlorosilanes, R_3SiCl and R_2SiCl_2. Among the products isolated was a family of four-membered diphosphadisiletanes, $(RPSiEt_2)_2$ (R = H, Ph, Me_3Si), and a novel trigonal bipyramidal cage compound, $P_2(SiEt_2)_3$. Since then, several research groups have contributed to the development of silaphosphane chemistry, and the formation of P–Si ring compounds and phosphorus rich cage and ladder compounds has been actively pursued.[2,3] However, additional examples of bicyclic and cage compounds in which *both* Si and P atoms are included in the core structure remain rare,[2,3] and their formation is still actively pursued.[4]

In a similar fashion, the synthesis of boraphosphane ring and cage compounds has attracted attention.[5] For example, in 1977, Fritz and Hölderich[6] noted that reaction of Me_2NBCl_2 with $LiP(SiMe_3)_2\cdot 2THF$ results in formation of a diphosphadiboretane, $(Me_2NBPSiMe_3)_2$, and our groups found that this reaction is generally applicable for synthesis of a family of diphosphadiboretanes, $(R_2NBPSiMe_3)_2$.[7] These rings are relatively unreactive toward ring coupling, and interest turned to the preparation of more reactive rings as well as transient multiply bonded fragments that should be useful starting materials for ring assembly approaches. In the course of that work, it was found that reactions of $LiPH_2\cdot DME$ with R_2NBCl_2 containing large amino groups usually produce diphosphadiboretanes, $(R_2NBPH)_2$, while R_2-

---

[†] University of New Mexico.

[‡] Universität München.

(1) Parshall, G. W.; Lindsay, R. V. *J. Am. Chem. Soc.* **1959**, *81*, 6273.

(2) Fritz, G. *Adv. Inorg. Chem.* **1987**, *31*, 171. Fritz, G.; Härer, J. *The Chemistry of Inorganic Homo- and Heterocycles*; Haiduc, I., Sowerby, D. B., Eds.; Academic Press: New York, 1987; Vol. I, Chapter 9 and references therein.

(3) Armitage, D. A. In *The Silicon-Heteroatom Bond*; Patai, S., Rappoport, Z., Eds.; J. Wiley: New York, 1991; Chapters 5 and 6 and references therein.

(4) Driess, M.; Pritzkow, H.; Reisgys, M. *Chem. Ber.* **1991**, *124*, 1923; **1991**, *124*, 1931 and references therein.

(5) Power, P. *Angew. Chem., Int. Ed. Engl.* **1990**, *29*, 449.

(6) Fritz, G.; Hölderich, W. *Z. Anorg. Allg. Chem.* **1977**, *431*, 61.

(7) Kölle, P.; Linti, G.; Nöth, H.; Wood, G. L.; Narula, C. K.; Paine, R. T. *Chem. Ber.* **1988**, *121*, 871.

0020-1669/93/1332-3056$04.00/0 © 1993 American Chemical Society

Scheme I

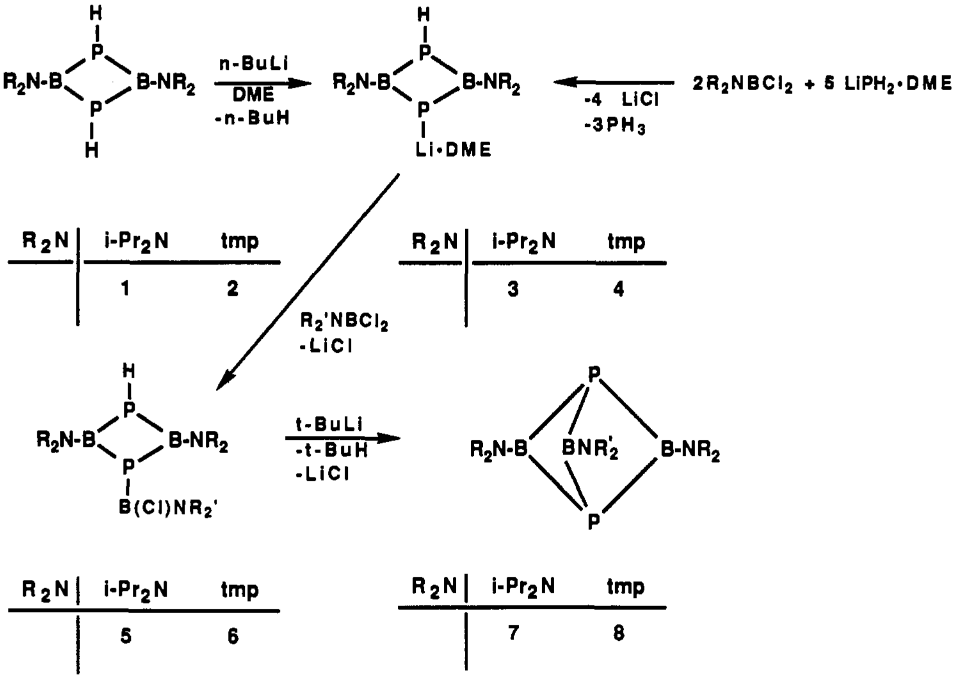

NBCl₂ compounds, having smaller amino groups ($R_2N = Me_2N$, Et_2N), give six-membered triphosphatriboretanes, $(R_2NBPH)_3$.[8,9] When R_2N = i-Pr_2N, both four-membered and six-membered rings are obtained. Further, it was observed that reaction of i-Pr_2NBCl_2 with i-$Pr_2NB(Cl)P(SiMe_3)_2$ led to formation of a novel trigonal bipyramidal cage compound, $P_2(BN$-i-$Pr_2)_3$.[10] Unfortunately, the last reaction is not general, so alternative routes to P_2B_3 rings were sought. A systematic approach has now been developed that is based on reaction of lithium salts $R_2NBP(H)B(NR_2)PLi{\cdot}DME$ with R'_2NBCl_2 followed by dehydrohalogenation with t-BuLi, as shown in Scheme I.[11] We describe here extensions of the stepwise assembly process to the synthesis of cage compounds containing boron, phosphorus, and silicon atoms.

Experimental Section

General Information. Standard inert-atmosphere techniques were used for the manipulation of all reagents and reaction products. Infrared spectra were recorded on a Matteson 2020 FT-infrared spectrometer from solution cells or KBr pellets. Mass spectra were obtained from a Finnegan mass spectrometer by using a GC inlet system or heated solids probe or by using a Kratos MS-50 spectrometer with FABS analysis. The latter mass spectral determinations were performed at the Midwest Center for Mass Spectrometry. NMR spectra were recorded on Bruker WP-250 and JEOL GSX-400 spectrometers. All NMR samples were sealed in 5-mm tubes with deuterated lock solvent, and the spectra were referenced with Me_4Si (^{13}C, ^1H), $BF_3{\cdot}Et_2O$ (^{11}B), and 85% H_3PO_4 (^{31}P). Elemental analyses were obtained from the UNM analytical services laboratory.

Materials. Reagents i-Pr_2NBCl_2,[12] $tmpBCl_2$,[13] $Me_2Si(Cl)Si(Cl)Me_2$,[14] $LiPH_2{\cdot}DME$,[15] the diphosphadiboretanes, $(i$-$Pr_2NBPH)_2$ (**1**) and $(tmpBPH)_2$ (**2**),[8] and their lithium salts **3** and **4**[8] were prepared as described in the literature. A modified synthesis for **3** is described below. The organylsilanes (Aldrich) and n-BuLi and t-BuLi solutions (Aldrich) were purchased and used as received. Solvents were dried and degassed by standard methods. Solvent transfers were accomplished by vacuum distillation, and all reactions and product workups were accomplished under dry nitrogen.

Synthesis and Characterization of Compounds 1-(Lithio·DME)-2,4-bis(diisopropylamino)-1,3,2,4-diphosphadiboretane (3). The yield of **3** can be improved over that described in the literature[8] by using the following procedure. A suspension of $LiPH_2{\cdot}DME$ (2.81 g, 21.6 mmol) in 10 mL of DME was cooled to −78 °C, and a solution containing 1.55 g (8.52 mmol) of i-Pr_2NBCl_2 in 20 mL of hexane was added dropwise with stirring. The resulting mixture was allowed to warm slowly over 2 h to 23 °C and stirred for an additional 15 h. The mixture was filtered, and colorless crystals deposited from the filtrate upon concentration and cooling to −10 °C. Yield: 1.32 g (81%).

Dipotassium Bis(2,4-bis(2,2,6,6-tetramethylpiperidino)-1,3,2,4-diphosphadiboretane) (9). A sample of $(tmpBPH)_2$ (0.77 g, 2.1 mmol) in 30 mL of benzene was added to 0.23 mL (4.2 mmol e⁻) of $K_{2.8}Na$, and the mixture was agitated for 1 h with a standard laboratory ultrasonicator. The $K_{2.8}Na$ alloy was completely consumed, and the resulting dark blue suspension containing $K_2P_2(Btmp)_2$ (**9**) was used in reactions without isolation.

2,4-Bis(diisopropylamino)-1-(dimethylphenylsilyl)-1,3,2,4-diphosphadiboretane (10). An excess (0.5 g, 2.9 mmol) of $Me_2(Ph)SiCl$ was dissolved in 25 mL of hexane and added to a hexane solution containing 1.0 g (2.6 mmol) of **3** held at 0 °C. The reaction mixture was stirred for 1 h, warmed to 23 °C, and stirred for 2 days. The resulting slurry was filtered and the solvent removed from the filtrate by vacuum evaporation. The remaining residue was recrystallized as a colorless crystalline solid from cold hexane: yield 0.8 g (73%); mp 99–101 °C. Mass spectrum (30 eV) [m/e (%)]: 420 (35, M^+), 284 (21, $M^+ - Me_2PhSi^+$), 253 (40), 188 (70), 135 (100), 110 (30). Infrared spectrum (hexane, cm⁻¹): 2263 (PH, w), 1454 (vs), 1443 (vs), 1429 (s), 1406 (w), 1366 (s), 1310 (s), 1256 (s), 1186 (s), 1148 (s), 1119 (s), 1070 (m), 1028 (w), 1007 (m), 835 (vs), 812 (vs), 768 (m), 698 (s), 660 (m), 498 (s), 471 (w). Anal. Calcd for $C_{20}H_{40}B_2N_2SiP_2$ (420.21): C, 57.17; H, 9.59; N, 6.67. Found: C, 56.91; H, 9.89; N, 6.52.

2,4-Bis(2,2,6,6-tetramethylpiperidino)-1-(dimethylphenylsilyl)-1,3,2,4-diphosphadiboretane (11). A sample (1.0 g, 2.2 mmol) of **4** was added to a solution containing excess (0.45 g, 2.6 mmol) $Me_2(Ph)SiCl$ at 0 °C. The reaction mixture was stirred at 0 °C for 2 h, warmed to 23 °C, stirred for an additional 16 h, and then heated at 50 °C for 16 h. The resulting yellow, cloudy solution was filtered and the solvent removed by vacuum evaporation. The solid residue was recrystallized twice from 20 mL of cold hexane, and colorless crystals were obtained: yield 1.0 g (49%); mp 94–96 °C. Mass spectrum (30 eV) [m/e (%)]: 500 (20, M^+), 333 (100), 160 (15), 135 (92). Infrared spectrum (hexane, cm⁻¹): 2226 (PH, m),

---

(8) Dou, D.; Westerhausen, M.; Wood, G. L.; Linti, G.; Duesler, E. N.; Nöth, H.; Paine, R. T. *Chem. Ber.* **1993**, *126*, 379.

(9) Linti, G.; Dou, D.; Duesler, E. N.; Paine, R. T.; Nöth, H. *Chem. Ber.*, submitted for publication.

(10) Wood, G. L.; Duesler, E. N.; Narula, C. K.; Paine, R. T.; Nöth, H. *J. Chem. Soc., Chem. Commun.* **1987**, 496.

(11) Dou, D.; Wood, G. L.; Duesler, E. N.; Paine, R. T.; Nöth, H. *Inorg. Chem.* **1992**, *31*, 3756.

(12) Gerrard, W.; Hudson, H. R.; Mooney, E. R. *J. Chem. Soc.* **1960**, 5168.

(13) Nöth, H.; Weber, S. *Z. Naturforsch., B* **1983**, *38*.

(14) Kumada, M.; Yamaguchi, M.; Yamamoto, Y.; Nakajima, J. I.; Shina, K. *J. Org. Chem.* **1956**, *21*, 1264.

(15) Schäfer, H.; Fritz, G.; Holderich, W. A. *Z. Anorg. Allg. Chem.* **1977**, *428*, 222.

Table I. Crystallographic Data for Compounds **15**, **17**, **20**, **21**, **23**, **24**, and **25**

	compound						
	15	**17**	**20**	**21**	**23**	**24**	**25**
chem formula	$C_{24}H_{38}B_2N_2P_2Si$	$C_{30}H_{46}B_2N_2P_2Si$	$C_{22}H_{48}B_2N_2P_2Si_2$	$C_{14}H_{35}B_2N_2P_2Si$	$C_{16}H_{40}B_2N_2P_2Si_2$	$C_{28}H_{38}B_2N_2O_4P_2SiFe$	$C_{24}H_{42}B_2N_2O_4P_2SiFe$
a (Å)	11.116(2)	14.445(9)	11.375(2)	10.994(2)	12.366(2)	14.403(3)	11.132(2)
b (Å)	11.436(2)	19.18(2)	14.977(2)	15.320(2)	13.377(2)	15.550(4)	32.531(9)
c (Å)	14.225(2)	23.25(2)	16.939(4)	13.389(3)	15.077(4)	15.632(3)	17.504(4)
α (deg)	67.280(10)						
β (deg)	67.660(10)			101.930(10)		102.070(10)	92.19(2)
γ (deg)	61.100(10)						
V (Å^3)	1417.78(44)	6428(6)	2885.7(10)	2206.4(7)	2494.1(9)	3423.5(10)	6334(3)
Z	2	8	4	4	4	4	8
ρ_{calcd} (g cm^{-3})	1.092	1.129	1.106	1.033	1.066	1.230	1.238
fw	466.2	546.3	480.4	343.1	400.2	634.1	590.1
cryst dimen (nm)	0.18 × 0.35 × 0.46	0.35 × 0.5 × 0.25	0.23 × 0.44 × 0.61	0.23 × 0.25 × 0.46	0.18 × 0.28 × 0.32	0.18 × 0.25 × 0.58	0.21 × 0.25 × 0.48
cryst syst	triclinic	orthorhombic	orthorhombic	monoclinic	orthorhombic	monoclinic	monoclinic
space group	$P\bar{1}$	*Pbca*	*Pnma*	$P2_1/n$	$P2_12_12_1$	$P2_1/n$	$P2_1/c$
T (°C)	20	20	20	20	20	20	20
μ (mm^{-1})	0.204	0.194	0.240	0.242	0.267	0.597	0.640
2θ range (deg)	2–45	3–44	2–50	2–45	2–47	2–50	2–45
reflcns measd	$\pm h,\pm k,\pm l$	$h,-k,l$	$-h,+k,\pm l$	$+h,\pm k,\pm l$	$+h,\pm k,\pm l$	$\pm h,-k,-l$	$+h,-k,\pm l$
tot. no. of reflcns collcd	7398	6435	5576	6127	7771	6520	8957
no. of unique reflcns	3702	3873	2646	2892	3687	6025	8259
no. of obsd reflcns	2733 ($F > 3\sigma(F)$)	2364 ($F > 2.5\sigma(F)$)	1423 ($F > 3\sigma(F)$)	2073 ($F > 3\sigma(F)$)	2586 ($F > 3\sigma(F)$)	3963 ($F > 3\sigma(F)$)	4759 ($F > 2\sigma(F)$)
transm coeff min/max	0.9023/0.9707		0.8912/0.9248	0.8636/0.8912	0.8048/0.8241	0.7620/0.8315	0.7989/0.8443
R_F	4.80	7.15	6.35	4.83	5.66	5.00	10.51
R_{wF}	4.26	5.51	5.05	3.91	4.37	4.77	8.47

Table II. Atomic Coordinates (×10^4) and Their Esd's for $P_2(i\text{-}Pr_2NB)_2(Ph_2Si)$ (**15**)

	x	*y*	*z*
P(1)	2886(1)	3742(1)	6666(1)
P(2)	1870(1)	4645(1)	8686(1)
B(1)	3630(4)	3831(4)	7679(3)
N(1)	5032(3)	3289(3)	7702(2)
C(1)	6190(4)	2671(5)	6847(3)
C(2)	7165(4)	3414(6)	6263(3)
C(3)	6954(5)	1128(5)	7233(4)
C(4)	5518(4)	3235(5)	8553(3)
C(5)	5136(5)	4639(6)	8643(4)
C(6)	5044(5)	2310(6)	9583(3)
B(2)	1760(4)	3377(4)	8126(3)
N(2)	1140(3)	2445(3)	8675(2)
C(7)	1237(4)	1412(4)	8232(3)
C(8)	2740(4)	416(4)	7907(3)
C(9)	478(5)	2098(5)	7349(4)
C(10)	301(4)	2401(4)	9777(3)
C(11)	1025(5)	1110(4)	10545(3)
C(12)	−1221(4)	2690(5)	9909(4)
Si	1448(1)	5764(1)	7081(1)
C(13)	−403(3)	6357(3)	7000(3)
C(14)	−675(4)	6302(4)	6147(3)
C(15)	−2039(5)	6727(4)	6065(3)
C(16)	−3146(5)	7228(5)	6834(4)
C(17)	−2933(5)	7312(6)	7674(4)
C(18)	−1569(4)	6859(5)	7761(3)
C(19)	2028(4)	7230(3)	6373(3)
C(20)	1060(4)	8586(4)	6160(3)
C(21)	1497(5)	9672(4)	5644(3)
C(22)	2896(6)	9436(5)	5320(3)
C(23)	3885(5)	8106(5)	5501(3)
C(24)	3455(4)	7028(4)	6020(3)

Table III. Atomic Coordinates (×10^4) and Their Esd's for $P_2(tmpB)_2(Ph_2Si)$ (**17**)

	x	*y*	*z*
P(1)	5439(1)	7211(1)	3414(1)
P(2)	3710(1)	7449(1)	4122(1)
Si	4579(1)	8164(1)	3584(1)
B(1)	4114(5)	6920(3)	3424(3)
B(2)	4997(4)	7118(3)	4224(3)
N(1)	3638(3)	6459(2)	3081(2)
N(2)	5428(3)	6820(2)	4701(2)
C(1)	5200(5)	8898(3)	3942(2)
C(2)	6055(6)	8814(4)	4213(3)
C(3)	6493(6)	9374(6)	4481(3)
C(4)	6078(9)	10020(5)	4489(4)
C(5)	5245(8)	10112(4)	4225(3)
C(6)	4812(5)	9558(4)	3959(3)
C(10)	2763(5)	6098(3)	3285(3)
C(11)	2573(5)	5436(4)	2941(3)
C(12)	2524(6)	5542(4)	2294(3)
C(13)	3127(5)	6122(4)	2095(3)
C(14)	3964(4)	6288(3)	2477(3)
C(15)	1931(4)	6591(3)	3259(3)
C(16)	2892(5)	5849(3)	3909(3)
C(17)	4431(4)	6906(3)	2186(2)
C(18)	4659(5)	5680(3)	2495(3)
C(20)	6238(5)	6327(3)	4639(3)
C(21)	6304(6)	5847(4)	5164(3)
C(22)	6325(6)	6169(4)	5739(3)
C(23)	5843(5)	6866(4)	5738(3)
C(24)	5058(5)	6977(4)	5300(2)
C(25)	7125(5)	6735(4)	4534(3)
C(26)	6069(5)	5823(3)	4136(3)
C(27)	4795(5)	7748(4)	5352(3)
C(28)	4225(5)	6521(4)	5437(3)
C(1A)	3957(6)	8511(3)	2934(3)
C(2A)	3022(6)	8351(3)	2829(3)
C(3A)	2616(6)	8532(4)	2313(4)
C(4A)	3099(8)	8871(4)	1896(4)
C(5A)	4006(7)	9052(3)	1996(3)
C(6A)	4428(5)	8870(3)	2513(3)

1427 (w), 1385 (m), 1370 (s), 1325 (vs), 1302 (s), 1244 (m), 1192 (w), 1169 (m), 1130 (m), 1105 (w), 1044 (w), 991 (m), 835 (m), 804 (s), 766 (w), 733 (w), 698 (m), 650 (w). Anal. Calcd for $C_{26}H_{48}B_2N_2SiP_2$ (500.34): C, 62.41; H, 9.67; N, 5.68. Found: C, 62.43; H, 9.64; N, 5.71.

2,4-Bis(diisopropylamino)-1-(chlorodiphenylsilyl)-1,3,2,4-diphosphadiboretane (12). A sample (0.65 g, 2.6 mmol) of Ph_2SiCl_2 was dissolved in 25 mL of hexane, and this solution was combined at −78 °C with 0.98 g (2.6 mmol) of **3** in 25 mL of hexane. The mixture was stirred at −78 °C for 1 h and then held at 23 °C for 16 h. The resulting white, cloudy mixture was filtered and the solvent removed from the filtrate by vacuum evaporation. The remaining slightly yellow oil crystallized from 20 mL of benzene, and one recrystallization from a minimum amount of benzene (∼5 mL) gave white crystals: yield 0.9 g (70%); mp 78–80 °C. Mass spectrum (30 eV) [*m/e* (%)]: 502 (40, M$^+$), 253 (30), 217 (30), 188 (50), 110 (40). Infrared spectrum (hexane, cm^{-1}): 2274 (PH, w), 1478 (w), 1445 (m), 1429 (w), 1368 (m), 1314 (s), 1186 (m), 1148 (m), 1109 (w), 1007 (w), 737 (w), 696 (m), 675 (m), 542 (w), 513 (w). Anal. Calcd for $C_{24}H_{39}B_2N_2SiP_2Cl$ (502.70): C, 57.34; H, 7.22; N, 5.57. Found: C, 56.55; H, 7.68; N, 5.32.

Table IV. Atomic Coordinates (×10^4) and Their Esd's for $P_2(tmpB)_2(Me_2Si\text{-}SiMe_2)$ (**20**)

	x	*y*	*z*
P	8411(1)	3499(1)	109(1)
Si	7571(1)	3281(1)	1298(1)
C(1)	6083(5)	3823(4)	1356(3)
C(2)	8477(5)	3777(4)	2108(3)
B(1)	9523(7)	2500	259(4)
N(1)	10760(5)	2500	287(3)
C(11)	11423(4)	3383(3)	209(3)
C(12)	12750(4)	3298(3)	385(3)
C(13)	13319(6)	2500	22(5)
C(14)	10967(5)	4054(3)	817(3)
C(15)	11271(5)	3756(3)	–623(3)
B(2)	7522(7)	2500	–370(4)
N(2)	6715(5)	2500	–995(3)
C(21)	6403(4)	3374(3)	–1404(3)
C(22)	5360(4)	3303(3)	–1978(3)
C(23)	5410(7)	2500	–2503(5)
C(24)	6030(4)	4081(3)	–795(3)
C(25)	7474(4)	3709(3)	–1871(3)

2,4-Bis(2,2,6,6-tetramethylpiperidino)-1-(chlorodimethylsilyl)-1,3,2,4-diphosphadiboretane (13). A sample (0.30 g, 2.3 mmol) of Me_2SiCl_2 was diluted in 50 mL of hexane, and this solution was combined at –78 °C with 1.1 g (2.3 mmol) of **4**. The reaction mixture was stirred at –78 °C for 2 h, warmed to 23 °C, and stirred for 20 h. The yellow, cloudy solution was filtered and the solvent removed from the filtrate by vacuum evaporation. The residue was recrystallized three times from 20 mL of hexane at –10 °C, and colorless crystals were isolated: yield 0.50 g (47%); mp 140–142 °C. Mass spectrum (30 eV) [*m*/*e* (%)]: 458 (M^+, 20), 333 (60), 271 (15), 182 (12), 150 (17), 82 (22). Infrared spectrum (cyclohexane, cm^{-1}): 2281 (PH, w), 2234 (w), 1382 (m), 1371 (s), 1364 (s), 1329 (vs), 1302 (m), 1245 (w), 1168 (w), 1129 (w), 1043 (w), 990 (w), 840 (w), 805 (m), 729 (w), 496 (vs). Anal. Calcd for $C_{20}H_{43}B_2N_2SiP_2Cl$ (458.69): C, 52.37; H, 9.45; N, 6.11. Found: C, 52.54; H, 9.74; N, 6.13.

2,4-Bis(2,2,6,6-tetramethylpiperidino)-1-(chlorodiphenylsilyl)-1,3,2,4-diphosphadiboretane (14). A sample (0.53 g, 1.1 mmol) of **4** in 25 mL of hexane was combined at –78 °C with a solution containing 0.29 g (1.1 mmol) of Ph_2SiCl_2 in 25 mL of hexane. The reaction mixture was stirred for 2 h at –78 °C, slowly warmed to 23 °C, and stirred for an additional 48 h. The resulting yellow, cloudy solution was filtered and the filtrate concentrated to ~5 mL. A white solid was isolated upon cooling the solution to –10 °C: yield 0.45 g, (68%); mp 187–189 °C. Mass spectrum (30 eV) [*m*/*e* (%)]: 395 (10), 364 (15), 333 (98), 217 (25), 154 (30), 69 (100). Infrared spectrum (hexane, cm^{-1}): 2239 (PH, w), 1460 (w), 1450 (w), 1429 (m), 1385 (m), 1364 (s), 1331 (vs), 1302 (m), 1244 (w), 1192 (w), 1169 (m), 1128 (m), 1105 (m), 1044 (w), 989 (m), 737 (w), 696 (s), 575 (w), 552 (w), 540 (w), 527 (w), 511 (m), 472 (w). Anal. Calcd for $C_{30}H_{47}B_2N_2SiP_2Cl$ (582.83): C, 61.82; H, 8.13; N, 4.81. Found: C, 59.33; H, 8.38; N, 4.96.

2,4-Bis(diisopropylamino)-5-diphenyl-1,3-diphospha-2,4-dibora-5-silabicyclo[1.1.1]pentane (15). A sample (1.2 g, 3.1 mmol) of **3** in 25 mL of hexane was added at –78 °C to a solution containing 0.8 g (3.1 mmol) of Ph_2SiCl_2 in 150 mL of hexane. After 1 h, the temperature was raised to 23 °C and the mixture stirred for 16 h. The white, cloudy solution was filtered and the filtrate cooled to –78 °C, and 2.0 mL of *t*-BuLi (1.6 M, in hexane) was added dropwise. The solution was stirred for 1 h at –78 °C and then warmed to 23 °C and held for 16 h. The yellow, cloudy solution was filtered and the solvent removed by vacuum evaporation. The yellow residue was recrystallized twice from 20 mL of hexane at –10 °C, and colorless crystals were isolated: yield 0.80 g (54%); mp 148–150 °C. Mass spectrum (30 eV) [*m*/*e* (%)]: 466 (M^+, 100), 188 (72), 144 (31), 104 (26). Infrared spectrum (hexane, cm^{-1}): 1441 (m), 1429 (m), 1366 (m), 1302 (s), 1186 (m), 1144 (m), 1109 (m), 1005 (w), 733 (w), 696 (m), 570 (w), 540 (m). Anal. Calcd for $C_{24}H_{38}B_2N_2SiP_2$ (466.24): C, 58.95; H, 8.33; N, 6.05. Found: C, 61.83; H, 8.22; N, 6.01.

2,4-Bis(2,2,6,6-tetramethylpiperidino)-5-dimethyl-1,3-diphospha-2,4-dibora-5-silabicyclo[1.1.1]pentane (16). Method a. A sample (1.0 g, 2.2 mmol) of **4** in 25 mL of hexane was added to a solution containing an excess (0.35 g, 2.7 mmol) of Me_2SiCl_2 in 100 mL of hexane at –78 °C. After being stirred for 2 days, the yellow, cloudy solution was filtered, the filtrate was cooled to –78 °C, and 1.3 mL of *t*-BuLi (1.7 M) was added slowly. The mixture was warmed to 23 °C, and after 16 h, the yellow-brown, cloudy solution was filtered. Solvent was removed by vacuum evaporation, and the yellow residue was recrystallized twice from 20 mL of hexane. Slightly yellow crystals were isolated: yield 0.50 g (55%); mp 151–153 °C. Mass spectrum (30 eV) [*m*/*e* (%)]: 422 (M^+, 100), 240 (32), 208 (9), 150 (10). Infrared spectrum (hexane, cm^{-1}): 1366 (s), 1327 (s), 1316 (s), 1292 (s), 1242 (w), 1163 (m), 1126 (w), 995 (m), 972 (w), 843 (m), 766 (w), 673 (m). Anal. Calcd for $C_{20}H_{42}B_2N_2SiP_2$ (422.23): C, 56.89; H, 10.03; N, 6.63. Found: C, 56.65; H, 10.22; N, 6.76.

Method b. A sample (0.94 g, 2.6 mmol) of $(tmpBPH)_2$ was used as described above to prepare a 2.6 mmol sample of $K_2P_2(Btmp)_2$ in 15 mL of benzene. A 0.31-mL (2.6 mmol) portion of Me_2SiCl_2 in 15 mL of benzene was dripped over 50 min into the stirred benzene solution of **9** held at 5 °C. The mixture was stirred overnight at room temperature, and the resulting slurry was filtered to remove KCl. The filtrate was vacuum evaporated, and light yellow crystals were recovered. Yield: 0.78 g (72%).

2,4-Bis(2,2,6,6-tetramethylpiperidino)-5-diphenyl-1,3-diphospha-2,4-dibora-5-silabicyclo[1.1.1]pentane (17). Method a. A sample (1.4 g, 3.0 mmol) of **4** in 25 mL of hexane was combined at 23 °C with a solution containing 0.76 g (3.0 mmol) of Ph_2SiCl_2 in 100 mL of hexane. The yellow, cloudy solution was filtered and the filtrate cooled to –78 °C. A solution (1.8 mL) of *t*-BuLi (1.7 M in pentane) was added dropwise, and the mixture was stirred for 2 h at –78 °C and for 16 h at 23 °C. The yellow, cloudy solution was filtered and the solvent removed by vacuum evaporation. The residue was recrystallized three times from 20 mL of hexane at –10 °C, and slightly yellow crystals were isolated: yield 1.0 g (61%); mp 192–194 °C. Mass spectrum (30 eV) [*m*/*e* (%)]: 546 (M^+, 100), 364 (10), 208 (20), 144 (10). Infrared spectrum (hexane, cm^{-1}): 1456 (w), 1429 (w), 1368 (s), 1331 (s), 1287 (w), 1256 (w), 1244 (w), 1171 (w), 1130 (w), 1099 (w), 995 (w), 972 (w), 735 (w), 698 (m), 554 (w), 513 (w). Anal. Calcd for $C_{30}H_{46}B_2N_2SiP_2$ (546.37): C, 65.95; H, 8.49; N, 5.13. Found: C, 63.56; H, 8.38; N, 5.01.

Method b. Prepared by analogy with **16** described in method b above from 0.33 g (0.9 mmol) of $(tmpBPH)_2$, 0.10 mL (1.80 mmol e^-) of $K_{2.8}Na$, and 0.19 mL (0.90 mmol) of Ph_2SiCl_2. The product was recrystallized from a pentane/toluene (80/20) solution at –35 °C. Yield: 0.36 g (74%) of colorless crystals.

2,4-Bis(2,2,6,6-tetramethylpiperidino)-5-(methylphenyl)-1,3-diphospha-2,4-dibora-5-silabicyclo[1.1.1]pentane (18). **18** was prepared in analogy with **16** described in method b above from 0.77 g (2.1 mmol) of $(tmpBPH)_2$, 0.23 mL of $K_{2.8}Na$ (4.2 mmol e^-), and 0.34 mL (2.1 mmol) of $Me(Ph)SiCl_2$. A yellow oil was recovered which was recrystallized from CH_2Cl_2 at –78 °C. Light yellow crystals were collected and characterized by NMR data: yield 0.79 g (75%); mp 189–190 °C.

2,4-Bis(2,2,6,6-tetramethylpiperidino)-1-(1-dimethyl-2-dimethyl-2-chlorodisilyl)-1,3,2,4-diphosphadiboretane (19). A sample (0.14 g, 0.75 mmol) of $Me_2(Cl)SiSi(Cl)Me_2$ in 25 mL of hexane was cooled to –78 °C and combined with 0.35 g (0.75 mmol) of **4**. The mixture was stirred at –78 °C for 2 h and at 23 °C for 16 h. The resulting mixture was filtered and the solvent removed by vacuum evaporation. The yellow, oily residue (0.36 g) was redissolved in a minimum of hexane; however, the product did not crystallize. All further attempts to obtain an analytically pure sample of **19** failed; however, the compound was characterized by NMR spectroscopy. This showed that **19** is contaminated with the cage compound $P_2(tmpB)_2(Si_2Me_4)$ (**20**).

2,4-Bis(2,2,6,6-tetramethylpiperidino)-5,6-dimethyl-1,3-diphospha-2,4-dibora-5,6-disilabicyclo[2.1.1]hexane (20). A sample (0.47 g, 2.5 mmol) of $Me_2(Cl)SiSi(Cl)Me_2$ was diluted with 25 mL of hexane and combined at –78 °C with a suspension of 1.16 g (2.5 mmol) of **4** in 25 mL of hexane. The mixture was stirred at –78 °C for 2 h, warmed to 23 °C, and stirred for an additional 16 h. The yellow, cloudy solution was filtered and the filtrate cooled to –78 °C. *t*-BuLi (1.5 mL, 1.7 M) was added slowly, and the mixture was stirred briefly at –78 °C, warmed to 23 °C, and stirred for 2 h. The yellow, cloudy solution was filtered and the filtrate concentrated to 5 mL. Yellow crystals deposited, and these were recrystallized from hexane: yield 0.70 g (58%); mp 207–209 °C. Mass spectrum (30 eV) [*m*/*e* (%)]: 480 (M^+, 100), 329 (84), 240 (8). Infrared spectrum (hexane, cm^{-1}): 1398 (w), 1385 (w), 1368 (m), 1314 (s), 1294 (s), 1240 (w), 1165 (w), 1128 (w), 1042 (w), 989 (w), 849 (w), 804 (w), 756 (w). Anal. Calcd for $C_{22}H_{48}B_2N_2Si_2P_2$ (480.39): C, 55.00; H, 10.07; N, 5.83. Found: C, 55.19; H, 10.11; N, 5.91.

1,2-Dimethyl-1,2-bis[2,4-bis(diisopropylamino)-1,3,2,4-diphosphadiboretanyl]disilane (21). A sample (2.4 g, 6.3 mmol) of **3** was dissolved in 50 mL of hexane and combined at 0 °C with 30 mL of hexane containing 0.59 g (3.2 mmol) of $Me_2(Cl)Si\text{–}Si(Cl)Me_2$. The mixture was stirred at 0 °C for 1 h and at 23 °C for 20 h. The white, cloudy solution was filtered and the solvent removed by vacuum evaporation. Colorless crystals were isolated following recrystallization of the residue from hexane at

−10 °C: yield 0.70 g (32%); mp 221–223 °C dec. Mass spectrum (30 eV) [*m/e* (%)]: 401 (100). Infrared spectrum (hexane, cm^{-1}): 2261 (PH, m), 1479 (m), 1441 (s), 1400 (w), 1368 (s), 1312 (vs), 1246 (s), 1186 (s), 1150 (s), 1115 (w), 1007 (m), 872 (w), 833 (s), 779 (vs), 667 (w), 650 (w), 577 (w), 492 (w), 469 (w). Anal. Calcd for $C_{28}H_{70}B_4N_4Si_2P_4$ (686.21): C, 49.01; H, 10.28; N, 8.16. Found: 48.79; H, 10.40; N, 8.06.

2,4-Bis(diisopropylamino)-5,6-dimethyl-1,3-diphospha-2,4-dibora-5,6-disilabicyclo[2.1.1]hexane (23). A sample (0.66 g, 1.0 mmol) of **21** was dissolved in 25 mL of THF, and 0.6 mL of *n*-BuLi (1.6 M in hexane) was added at −78 °C. The mixture was stirred for 2 h at −78 °C and for 16 h at 23 °C. After the mixture, evaporated to dryness, the residue was redissolved in 50 mL of hexane. To this solution was added 0.18 g (0.96 mmol) of $Me_2(Cl)Si–Si(Cl)Me_2$ in 25 mL of hexane at −78 °C. The reaction mixture was stirred for 2 h, warmed to 23 °C, and stirred for an additional 16 h. The yellow, cloudy solution was then filtered and cooled to −78 °C, and *t*-BuLi (0.56 mL, 1.7 M in pentane) was added by syringe. The solution became cloudy upon addition, and it was stirred briefly at −78 °C. The mixture was then warmed to 23 °C and stirred for an additional 16 h. The cloudy solution was filtered and concentrated to 5 mL. A yellow solid deposited upon cooling the solution to −10 °C. This material was recrystallized from 20 mL of cold hexane, leaving a white crystalline solid: yield 0.35 g (45%); mp 170–172 °C. Mass spectrum (30 eV) [*m/e* (%)]: 400 (M$^+$, 100). Infrared spectrum (hexane, cm^{-1}): 1478 (w), 1439 (m), 1400 (w), 1368 (m), 1302 (s), 1238 (w), 1186 (m), 1146 (m), 1111 (w), 1005 (w), 849 (w), 829 (w), 802 (m), 754 (w), 725 (w), 669 (w), 644 (w), 573 (w), 496 (w). Anal. Calcd for $C_{16}H_{40}B_2N_2Si_2P_2$ (400.25): C, 48.01; H, 10.07; N, 7.00. Found: C, 48.12; H, 10.30; N, 7.16.

Complexes. The syntheses of the complexes **24**–**28** were performed in the following fashion. Ligands **15**, **16**, **17**, **20**, or **23** (1 mmol) and $Fe_2(CO)_9$ (1 mmol) were combined in 50 mL of hexane and the resulting solutions stirred for 2–3 days. The mixtures were filtered, the filtrates evaporated to dryness, and the residues recrystallized from hexane at −10 °C.

Characterization. $P_2[i\text{-}Pr_2NB]_2(Ph_2Si)\cdot Fe(CO)_4$ (24). Orange crystals: yield 59%; mp 160–162 °C dec. Mass spectrum (30 eV) [*m/e* (%)]: 550 (3), 522 (100), 188 (70), 144 (15). Infrared spectrum (hexane, cm^{-1}): 2041 (s), 1968 (s), 1937 (vs), 1479 (w), 1369 (w), 1321 (w), 1114 (w), 698 (w), 621 (m). Anal. Calcd for $C_{28}H_{38}B_2N_2O_4SiP_2Fe$ (634.13): C, 53.03; H, 6.68; N, 4.42. Found: C, 51.88; H, 6.14; N, 4.32.

$P_2(tmpB)_2(Me_2Si)\cdot Fe(CO)_4$ (25). Yellow crystals: yield 80%; mp 178–180 °C dec. Mass spectrum (30 eV) [*m/e* (%)]: 562 (M$^+$ − CO, 0.9), 534 (14), 478 (100), 422 (38), 364 (20), 325 (72), 203 (18). Infrared spectrum (hexane, cm^{-1}): 2037 (s), 1964 (s), 1931 (vs), 1387 (w), 1248 (w), 1173 (w), 1128 (w), 976 (w), 845 (w). Anal. Calcd for $C_{24}H_{42}B_2N_2O_4SiP_2Fe$ (590.12): C, 48.85; H, 7.17; N, 4.75. Found: C, 48.74; H, 7.71; N, 6.19.

$P_2(tmpB)_2(Ph_2Si)\cdot Fe(CO)_4$ (26). Yellow crystals: yield 57%; mp 177–180 °C dec. Mass spectrum (30 eV) [*m/e* (%)]: 546 (70), 364 (35), 235 (23), 207 (82). Infrared spectrum (hexane, cm^{-1}): 2039 (s), 1964 (s), 1937 (vs), 1429 (w), 1387 (w), 1344 (w), 1173 (w), 1128 (w), 698 (w), 623 (m), 515 (w). Anal. Calcd for $C_{34}H_{46}B_2N_2O_4SiP_2Fe$ (714.26): C, 57.17; H, 6.49; N, 3.92. Found: C, 56.37; H, 6.87; N, 6.23.

$P_2(tmpB)_2(Me_2Si)_2\cdot Fe(CO)_4$ (27): Brown crystals: yield 73%; mp 160–162 °C dec. Mass spectrum (30 eV) [*m/e* (%)]: 592 (M$^+$ − 2CO, 5), 536 (12), 480 (100), 422 (41), 329 (48), 240 (8). Infrared spectrum (hexane, cm^{-1}): 2033 (m), 2004 (w), 1940 (vs), 1385 (w), 1368 (w), 1325 (w), 1296 (w), 1244 (w), 1167 (w), 1128 (w), 1043 (w), 991 (w), 847 (w), 826 (w), 804 (w), 787 (w), 772 (w), 727 (w), 638 (w), 621 (w). Anal. Calcd for $C_{26}H_{48}B_2N_2O_4Si_2P_2Fe$ (648.28): C, 48.17; H, 7.46; N, 4.32. Found: C, 47.83; H, 7.27; N, 4.28.

$P_2[(i\text{-}Pr_2NB)_2](Me_2Si)_2\cdot Fe(CO)_4$ (28). Brown crystals: yield 45%; mp 204–206 dec. Mass spectrum (30 eV) [*m/e* (%)]: 568 (M$^+$, 6), 512 (M − 2CO$^+$, 57), 484 (M − 3CO$^+$, 85), 456 (M − 4CO$^+$, 33). Infrared spectrum (hexane, cm^{-1}): 2033 (s), 1958 (s), 1925 (s), 1369 (w), 1315 (m), 1246 (w), 1184 (w), 1148 (w), 1113 (w), 1086 (w), 1032 (w), 1001 (w), 851 (w), 831 (w), 802 (w). Anal. Calcd for $C_{20}H_{40}B_2N_2O_4Si_2P_2Fe$ (568.14): C, 42.28; H, 7.10; N, 4.93. Found: C, 42.30; H, 7.50; N, 4.99.

Crystallographic Measurements and Structure Solutions. Crystals of **15**, **17**, **20**, **21**, **23**, **24**, and **25** were placed in glass capillaries under a dry nitrogen atmosphere. The crystals were centered on a Syntex P3/F automated diffractometer, and determinations of crystal class, orientation matrix, and unit cell dimensions were performed in a standard manner. A summary of crystallographic data is given in Table I. Data were collected in the ω scan mode with Mo/Kα (λ = 0.710 69 Å) radiation, a scintillation counter, and pulse height analyzer. In each case, inspection of a small data set led to assignment of the indicated space groups.[16] With exception of **17**, empirical adsorption corrections were applied, based on ψ scans.[17] No signs of crystal decay were noted.

Table V. Atomic Coordinates (×10^4) and Their Esd's for $i\text{-}Pr_2NBP(H)B(N\text{-}i\text{-}Pr_2)PSi(Me_2)Si(Me_2)PB(i\text{-}Pr_2N)P(H)BNi\text{-}Pr_2$ (**21**)

	x	*y*	*z*
Si	−5656(9)	44591(6)	3157(7)
P(1)	−7715(9)	47508(6)	19279(7)
P(2)	3400(10)	63029(6)	29087(9)
B(1)	7408(37)	50824(26)	28809(29)
B(2)	−12545(41)	59394(27)	21578(31)
N(1)	17168(27)	45786(18)	33698(20)
N(2)	−24009(28)	63525(19)	18736(22)
C(1)	26674(37)	48710(27)	42626(31)
C(2)	34238(41)	56307(33)	40006(37)
C(3)	20869(44)	50683(29)	51682(30)
C(4)	18403(39)	36644(25)	30459(29)
C(5)	16948(49)	30144(28)	38587(35)
C(6)	30443(44)	35255(32)	26622(37)
C(7)	−26614(41)	72471(26)	22024(29)
C(8)	−25231(42)	73043(27)	33525(29)
C(9)	−18862(47)	79262(28)	18001(37)
C(10)	−34731(37)	58850(29)	12635(30)
C(11)	−44613(36)	56919(34)	18959(34)
C(12)	−40341(41)	63545(32)	2646(31)
C(13)	−21582(30)	43906(25)	−5088(25)
C(14)	2098(35)	33735(22)	2848(26)

All calculations were performed on Siemens SHELXTL PLUS (Microvax II and PC versions) structure determination systems.[18] Solutions for the data sets were by direct methods, and full matrix refinements were employed.[19] Neutral-atom scattering factors and anomalous dispersion terms were used for all non-hydrogen atoms during the refinements. The function minimized was $\sum w(|F_o| - |F_c|)^2$. Listings of the non-hydrogen atom coordinates are given in Tables II–VIII, and selected bond distances and angles are summarized in Table IX. Additional crystallographic data and details of the structure solutions (Table S-1), hydrogen atom positional parameters (Table S-2), anisotropic thermal parameters (Table S-3), and full listings of bond distances and angles (Table S-4) are provided in the supplementary material.

Results and Discussion

As outlined in the Introduction, the goal of the present study was to determine if diphosphadiboretanes can be employed as synthons to form $P_2(BNR_2)_2E_x$ (E = Si) cages. Two approaches were used to obtain the required phosphido anions. The first approach directly extends the previously reported[11] reaction chemistry summarized in Scheme I. The lithium salts **3** and **4** are prepared via deprotonation reactions, as described in eqs 1 and 2. We have previously reported[8] that **3** is formed in good yield from a one-pot 5:2 stoichiometric combination of $LiPH_2\cdot DME$ and $i\text{-}Pr_2NBCl_2$ in hexane, while **4** is best obtained by deprotonation of the isolated diphosphadiboretane $(tmpBPH)_2$ **2** with *n*-BuLi. It is further found here that **3** is obtained reliably in better yield when the reaction described in eq 1 is performed in a mixed solvent system of DME and hexane (1:2).

---

(16) Space group notation as given in: *International Tables for X-Ray Crystallography*; Reidel: Dordrecht, Holland, 1983, Vol. I, pp 73–346.

(17) The empirical absorption corrections use an ellipsoidal model fitted to azimuthal scan data that are then applied to the intensity data: *SHELXTL Manual, Revision 4*, Nicolet XRD Corp.: Madison, WI, 1983.

(18) Sheldrick, G. M. *Nicolet SHELXTL Operations Manual*; Nicolet XRD Corp.: Cupertino, CA, 1981. SHELXTL uses absorption, anomalous dispersion, and scattering data compiled in: *International Tables for X-Ray Crystallography*, Kynoch: Birmingham, England, 1974; Vol. IV, pp 55–60, 99–101, 149–150. Anomalous dispersion terms were included for all atoms with atomic numbers greater than 2.

(19) A general description of the least-squares algebra is found in: *Crystallographic Computing*; Ahmed, F. R., Hall, S. R., Huber, C. P., Eds.; Munksgaard: Copenhagen, 1970; p 187. The least-squares refinement minimizes $\sum w(|F_o| - |F_c|)^2$, where $w = 1/[\sigma(F)^2 + gF^2]$. $R = \sum||F_o| - |F_c||/\sum|F_o|$, $R_{wF} = [\sum(|F_o| - |F_c|)^2/\sum wF_o^2]$, and GOF $= [\sum_w(|F_o| - |F_c|)^2/(NO - NV)]^{1/2}$, where NO = number of observations and NV = number of variables.

Table VI. Atomic Coordinates (×10^4) and Their Esd's for P_2(i-$Pr_2NB)_2(MeSi–SiMe_2)$ (**23**)

	x	*y*	*z*
P(1)	3187(1)	1876(1)	7222(1)
P(2)	1777(1)	−11(1)	7228(1)
B(1)	3314(5)	404(4)	7225(4)
N(1)	4245(3)	−147(3)	7311(3)
C(1)	5319(4)	350(4)	7361(5)
C(2)	6077(5)	40(5)	6619(4)
C(3)	5836(5)	215(5)	8264(4)
C(4)	4286(5)	−1263(4)	7374(4)
C(5)	3719(5)	−1648(4)	8196(4)
C(6)	3902(5)	−1759(4)	6543(4)
B(2)	1713(5)	1422(4)	7545(4)
N(2)	888(3)	1912(3)	7976(3)
C(7)	960(5)	2945(4)	8337(4)
C(8)	1777(5)	3013(4)	9085(4)
C(9)	1183(4)	3715(4)	7612(4)
C(10)	−152(4)	1395(4)	8153(4)
C(11)	−1126(4)	1953(5)	7759(4)
C(12)	−316(5)	1178(5)	9133(5)
Si(1)	2749(1)	1807(1)	5761(1)
C(13)	2197(5)	3016(4)	5343(4)
C(14)	3990(5)	1501(5)	5085(4)
Si(2)	1537(1)	452(1)	5800(1)
C(15)	1873(5)	−573(4)	4991(4)
C(16)	87(4)	807(4)	5631(4)

Table VII. Atomic Coordinates (×10^4) and Their Esd's for P_2(i-$Pr_2NB)_2(Ph_2Si)\cdot Fe(CO)_4$ (**24**)

	x	*y*	*z*
Fe	2329(1)	8700(1)	5222(1)
C(1)	1644(4)	9659(3)	5177(3)
O(1)	1216(3)	10272(3)	5159(2)
C(2)	3112(3)	9067(3)	6188(3)
O(2)	3604(3)	9323(2)	6811(2)
C(3)	2580(3)	8912(3)	4174(3)
O(3)	2713(3)	9080(2)	3491(2)
C(4)	1328(4)	8033(3)	5248(3)
O(4)	677(3)	7614(3)	5264(3)
Si	3190(1)	6291(1)	4501(1)
C(5)	3513(3)	6489(3)	3420(2)
C(6)	3414(3)	5851(3)	2790(3)
C(7)	3664(4)	5999(4)	1995(3)
C(8)	4020(3)	6774(4)	1815(3)
C(9)	4130(3)	7419(3)	2427(3)
C(10)	3871(3)	7274(3)	3222(3)
C(11)	2114(3)	5593(3)	4376(3)
C(12)	1980(3)	5041(3)	5037(3)
C(13)	1200(4)	4497(3)	4934(4)
C(14)	550(4)	4496(4)	4178(4)
C(15)	640(5)	5039(5)	3530(4)
C(16)	1422(4)	5582(4)	3623(3)
P(1)	3228(1)	7479(1)	5339(1)
P(2)	4398(1)	5933(1)	5610(1)
B(1)	4580(3)	7174(3)	5447(3)
B(2)	3543(3)	6568(3)	6222(3)
N(1)	5377(2)	7653(2)	5456(2)
N(2)	3341(2)	6480(2)	7038(2)
C(17)	5344(3)	8606(3)	5395(3)
C(18)	5738(4)	8941(3)	4627(4)
C(19)	5823(4)	9012(4)	6254(4)
C(20)	6343(3)	7270(3)	5532(4)
C(21)	6377(4)	6730(4)	4726(4)
C(22)	6660(3)	6780(4)	6381(4)
C(23)	3786(4)	5817(3)	7689(3)
C(24)	4854(4)	5984(4)	8003(3)
C(25)	3581(4)	4907(3)	7367(3)
C(26)	2681(3)	7074(3)	7343(3)
C(27)	3156(4)	7587(4)	8155(3)
C(28)	1789(4)	6613(4)	7480(4)

In an alternative approach, it is found that $K_{2.8}Na$ alloy deprotonates *both* phosphane centers in **2**, leaving a very reactive dipotassium salt **9** as summarized in eq 3. Although the precise nature of this salt has not yet been determined, several reactions with substrates have been examined, as described below. Attempts to prepare the bimetallated salt of **1** with $K_{2.8}Na$ have so far been unsuccessful.

Table VIII. Atomic Coordinates (×10^4) and Their Esd's for $P_2(tmpB)_2(Me_2Si)\cdot Fe(CO)_4$ (**25**)

	x	*y*	*z*
Fe(1)	4711(1)	5935(1)	9082(1)
C(1)	3466(12)	5728(4)	8541(8)
O(1)	2677(9)	5594(3)	8210(6)
C(2)	4462(12)	6423(5)	8659(7)
O(2)	4232(10)	6726(3)	8354(6)
C(3)	5697(12)	5581(4)	8681(8)
O(3)	6309(9)	5325(3)	8425(7)
C(4)	4037(11)	5799(4)	9955(7)
O(4)	3561(8)	5701(3)	10490(6)
P(1)	6332(3)	6137(1)	9874(2)
B(1)	6602(12)	6466(4)	10825(7)
N(1)	6007(8)	6751(3)	11232(5)
C(5)	6398(11)	6842(4)	12060(7)
C(6)	5364(13)	7065(5)	12456(8)
C(7)	4907(13)	7456(5)	12088(8)
C(8)	5047(11)	7453(4)	11225(7)
C(9)	5039(13)	7016(4)	10884(8)
C(10)	6593(11)	6443(4)	12497(7)
C(11)	7543(11)	7108(4)	12087(7)
C(12)	5366(20)	7093(5)	10054(8)
C(13)	3884(13)	6816(5)	10901(14)
B(2)	8074(12)	6292(4)	9878(8)
N(2)	8889(8)	6424(3)	9361(5)
C(14)	8579(12)	6512(4)	8534(8)
C(15)	9383(15)	6836(7)	8205(10)
C(16)	10685(17)	6765(6)	8288(11)
C(17)	10993(15)	6504(8)	8868(13)
C(18)	10211(17)	6485(6)	9626(10)
C(19)	7393(15)	6738(5)	8445(9)
C(20)	8456(20)	6134(6)	8086(10)
C(21)	10665(13)	6117(6)	10038(11)
C(22)	10273(14)	6866(6)	10099(10)
P(2)	8242(3)	6232(1)	11001(2)
Si(1)	7212(3)	5670(1)	10652(2)
C(23)	8057(12)	5260(4)	10172(8)
C(24)	6218(12)	5442(4)	11356(7)
Fe(2)	85(2)	3352(1)	4661(1)
C(25)	1198(13)	3149(4)	4080(8)
O(5)	1941(10)	3019(3)	3705(7)
C(26)	430(12)	3847(5)	4299(8)
O(6)	721(10)	4158(3)	4065(7)
C(27)	−1031(13)	3028(4)	4244(8)
O(7)	−1713(10)	2791(3)	3991(7)
C(28)	847(13)	3140(4)	5482(8)
O(8)	1346(10)	2989(3)	5987(6)
P(3)	−1365(3)	3615(1)	5451(2)
N(3)	−1094(8)	4324(3)	6667(5)
C(29)	205(10)	4444(3)	6534(7)
C(30)	771(13)	4644(5)	7247(9)
C(31)	114(14)	5027(5)	7514(9)
C(32)	−1136(18)	5013(6)	7347(14)
C(33)	−1787(12)	4619(4)	7198(8)
C(34)	963(11)	4060(4)	6435(7)
C(35)	267(12)	4703(4)	5824(7)
C(36)	−2966(13)	4746(5)	6807(9)
C(37)	−1997(13)	4388(5)	7906(8)
B(3)	−1672(11)	3995(4)	6307(7)
B(4)	−3094(12)	3756(4)	5357(8)
N(4)	−3918(8)	3880(3)	4769(5)
C(38)	−3539(11)	4041(4)	4014(7)
C(39)	−4482(11)	4338(4)	3667(8)
C(40)	−5701(14)	4143(5)	3532(9)
C(41)	−5960(12)	3806(4)	4110(7)
C(42)	−5281(12)	3859(4)	4897(8)
C(43)	−2403(12)	4306(4)	4134(8)
C(44)	−3269(13)	3701(4)	3462(8)
C(45)	−5690(13)	4231(5)	5321(8)
C(46)	−5553(12)	3464(4)	5322(7)
P(4)	−3281(3)	3765(1)	6463(2)
Si(2)	−2142(3)	3206(1)	6344(2)
C(47)	−1157(11)	3081(4)	7182(7)
C(48)	−2887(11)	2738(4)	5939(7)

The monolithium salts **3** and **4** are reactive toward monochlorosilanes such as $PhMe_2SiCl$, and P-monosilylated diphosphadiboretanes $R_2N\overline{BP(H)B(NR_2)P}SiMe_2Ph$ (**10, 11**) are obtained as crystalline solids, as described in eq 4. These compounds are

Table IX. Selected Bond Distances (Å) and Bond Angles (deg) for **15**, **17**, **20**, **21**, **23**, **24**, and **25**

	15		**17**		**20**		**21**		**23**		**24**		**25**			
							Bond Lengths									
B–P	1.969(6)	P(1)–B(1)	1.992(7)	P(1)–B(1)	1.976(5)	P–B(1)	1.942(4)	P(1)–B(1)	1.975(6)	P(1)–B(1)	1.977(5)	P(1)–B(1)	1.994(13)	P(1)–B(1)		
	1.978(4)	P(1)–B(2)	1.996(7)	P(1)–B(2)	1.980(5)	P–B(2)	1.939(4)	P(1)–B(2)	1.982(6)	P(1)–B(2)	1.964(5)	P(1)–B(2)	2.004(13)	P(1)–B(2)		
	1.971(4)	P(2)–B(1)	2.002(7)	P(2)–B(1)	1.976(5)	P′–B(1)	1.923(4)	P(2)–B(1)	1.980(6)	P(2)–B(1)	1.971(5)	P(2)–B(1)	1.992(13)	P(2)–B(1)		
	1.974(6)	P(2)–B(2)	1.979(7)	P(2)–B(2)	1.980(5)	P′–B(2)	1.914(4)	P(2)–B(2)	1.977(6)	P(2)–B(2)	1.975(5)	P(2)–B(2)	1.978(14)	P(2)–B(2)		
													1.985(13)	P(3)–B(3)		
													1.979(13)	P(3)–B(4)		
													1.970(13)	P(4)–B(3)		
													1.955(14)	P(4)–B(4)		
P–Si	2.239(1)	P(1)–Si	2.245(3)	P(1)–Si	2.254(2)	P–Si	2.261(1)	P(1)–Si	2.269(2)	P(1)–Si(1)	2.259(2)	P(1)–Si	2.242(5)	P(1)–Si(1)		
	2.248(1)	P(2)–Si	2.241(3)	P(1)–Si					2.261(2)	P(2)–Si(2)	2.254(2)	P(2)–Si	2.231(5)	P(2)–Si(1)		
													2.250(5)	P(3)–Si(2)		
													2.232(5)	P(4)–Si(2)		
B–N	1.379(5)	B(1)–N(1)	1.374(8)	B(1)–N(1)	1.407(9)	B(1)–N(1)	1.373(5)	B(1)–N(1)	1.373(5)	B(1)–N(1)	1.367(6)	B(1)–N(1)	1.356(16)	B(1)–N(1)		
	1.371(6)	B(2)–N(2)	1.394(8)	B(2)–N(2)	1.400(9)	B(2)–N(2)	1.391(7)	B(2)–N(2)	1.375(7)	B(2)–N(2)	1.372(6)	B(2)–N(2)	1.374(16)	B(2)–N(2)		
													1.385(15)	B(3)–N(3)		
													1.410(15)	B(4)–N(4)		
Si–C	1.865(4)	Si–C(13)	1.865(7)	Si–C(1)	1.879(6)	Si–C(1)	1.870(3)	Si(1)–C(13)	1.865(6)	Si–C(13)	1.870(4)	Si–C(5)	1.851(15)	Si(1)–C(23)		
	1.867(4)	Si–C(19)	1.879(7)	Si–C(1A)	1.869(6)	Si–C(2)	1.873(4)	Si(1)–C(14)	1.888(6)	Si–C(14)	1.868(4)	Si–C(11)	1.843(14)	Si(1)–C(24)		
									1.881(6)	Si–C(15)			1.844(12)	Si(2)–C(47)		
									1.872(5)	Si(2)–C(16)			1.861(12)	Si(2)–C(48)		
Si–Si					2.339(3)		2.333(2)		2.352(2)							
Fe–P											2.283(1)		2.328(3)	Fe(1)–P(1)		
													2.327(4)	Fe(2)–P(3)		
Fe–CO											1.782(5)	Fe–C(1)	1.781(13)	Fe(1)–C(1)		
											1.780(4)	Fe–C(2)	1.767(15)	Fe(1)–C(2)		
											1.781(5)	Fe–C(3)	1.756(14)	Fe(1)–C(3)		
											1.783(5)	Fe–C(4)	1.783(13)	Fe(1)–C(4)		
													1.762(14)	Fe(2)–C(25)		
													1.776(16)	Fe(2)–C(26)		
													1.766(14)	Fe(2)–C(27)		
													1.781(14)	Fe(2)–C(28)		
							Bond Angles									
B–P–B	67.3(2)	B(1)–P(1)–B(2)	70.0(3)	B(1)–P(1)–B(2)	78.9(3)	B(1)–P–B(2)	82.8(2)	B(1)–P(1)–B(2)	76.5(2)	B(1)–P(1)–B(2)	71.8(2)	B(1)–P(1)–B(2)	75.3(5)	B(1)–P(1)–B(2)		
	67.3(2)	B(1)–P(2)–B(2)	70.2(3)	B(1)–P(2)–B(2)			84.0(2)	B(1)–P(2)–B(2)	76.5(2)	B(1)–P(2)–B(2)	71.7(2)	B(1)–P(2)–B(2)	75.9(5)	B(1)–P(2)–B(2)		
													73.9(5)	B(3)–P(3)–B(4)		
													74.8(5)	B(3)–P(4)–B(4)		
P–B–P	101.5(2)	P(1)–B(1)–P(2)	98.5(3)	P(1)–B(1)–P(2)	98.5(4)	P–B(1)–P′			101.7(3)	P(1)–B(1)–P(2)	95.2(2)	P(1)–B(1)–P(2)	91.8(6)	P(1)–B(1)–P(2)		
	101.0(2)	P(1)–B(2)–P(2)	99.1(3)	P(1)–B(2)–P(2)	98.2(4)	P–B(2)–P′			101.6(3)	P(1)–B(2)–P(2)	95.5(2)	P(1)–B(2)–P(2)	91.9(6)	P(1)–B(2)–P(2)		
													92.9(5)	P(3)–B(3)–P(4)		
													93.5(6)	P(3)–B(4)–P(4)		
P–Si–P	85.7(1)	P(1)–Si–P(2)	84.8(1)	P(1)–Si–P(2)			95.7(2)	P(1)–B(1)–P(2)	99.2(1)	P(1)–Si(1)–Si(2)						
							96.1(2)	P(1)–B(2)–P(2)	98.7(1)	P(2)–Si(2)–Si(1)						
P–Si–Si′					98.3(1)								80.5(1)	P(1)–Si–P(2)	79.6(2)	P(1)–Si(1)–P(2)
													79.5(2)	P(3)–Si(2)–P(4)		
B–P–Si	73.8(1)	B(1)–P(1)–Si	72.2(2)	B(1)–P(1)–Si	92.7(2)	B(1)–P–Si			88.9(2)	B(1)–P(1)–Si(1)						
	71.5(1)	B(2)–P(1)–Si	74.3(2)	B(2)–P(1)–Si	92.3(2)	B(2)–P–Si			90.4(2)	B(2)–P(1)–Si(1)						
	73.6(1)	B(1)–P(2)–Si	72.2(2)	B(1)–P(2)–Si					92.7(2)	B(1)–P(2)–Si(2)						
	71.4(1)	B(2)–P(2)–Si	74.8(2)	B(2)–P(2)–Si					87.7(2)	B(2)–P(2)–Si(2)	75.9(1)	B(1)–P(1)–Si	79.0(4)	B(1)–P(1)–Si(1)		
							111.8(1)				77.9(1)	B(2)–P(1)–Si	76.6(4)	B(2)–P(1)–Si(1)		
											76.2(1)	B(1)–P(2)–Si	79.3(4)	B(1)–P(2)–Si(1)		
							116.0(1)	B(1)–P(1)–Si			77.9(1)	B(2)–P(2)–Si	77.4(4)	B(2)–P(2)–Si(1)		
							115.0(1)	B(2)–P(1)–Si					76.2(4)	B(3)–P(3)–Si(2)		
													78.3(4)	B(4)–P(3)–Si(2)		
													77.0(4)	B(3)–P(4)–Si(2)		
													79.2(4)	B(4)–P(4)–Si(2)		

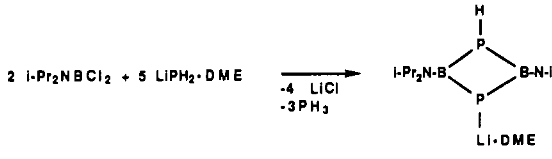

3

(1)

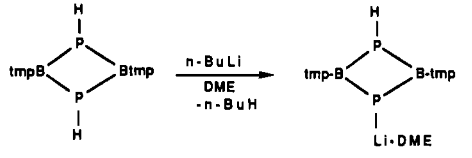

2 **4**

(2)

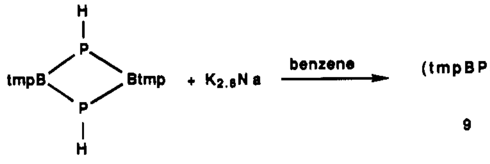

9

2

(3)

stable toward alkane elimination up to 100 °C; therefore, they are not directly useful for cage closure chemistry.

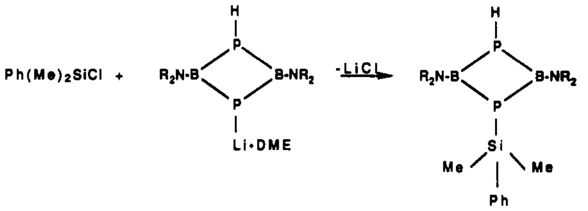

(4)

	3	**4**
R2N	i-Pr2N	tmp

	10	**11**
R2N	i-Pr2N	tmp

The reactions of **3** and **4** with Ph_2SiCl_2 and **4** with Me_2SiCl_2 result in formation of more reactive P-monosilylated diphosphadiboretanes **12–14** as summarized in eq 5. Subsequent dehydrohalogenation of these compounds, promoted with *t*-BuLi, proceeds smoothly, as shown in eq 6, with formation of bicyclic, trigonal bipyramidal cage compounds $P_2(BNR_2)_2SiR'_2$ (**15–17**) isolated as pure crystalline solids. The reaction of **3** with Me_2SiCl_2 was also studied. The reaction proceeds smoothly, but all attempts to isolate the product $i\text{-}Pr_2N\overline{BP(H)B(i\text{-}Pr_2N)P}SiMe_2Cl$ in pure form failed.

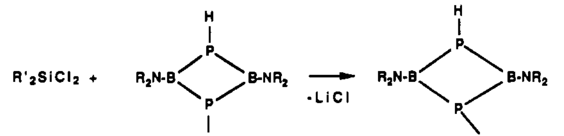

(5)

	12	**13**	**14**
R2N	i-Pr2N	tmp	tmp
R2'Si(Cl)	Ph2Si(Cl)	Me2Si(Cl)	Ph2Si(Cl)

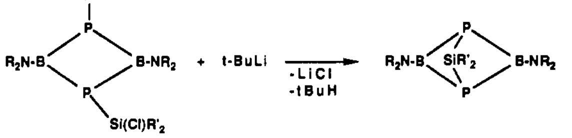

(6)

	15	**16**	**17**
R2N	i-Pr2N	tmp	tmp
R2'Si	Ph2Si	Me2Si	Ph2Si

The combinations of the dipotassium salt $(tmpBPK)_2$ (**9**) with dichlorosilanes Me_2SiCl_2, Ph_2SiCl_2, and $PhMeSiCl_2$ also give the bicyclic compounds **16–18**, as described in eq 7. Both synthetic routes to the bicyclic compounds provide good yields; however, the present inability to form the bimetallic salt of **1** limits the utility of the one-step approach.

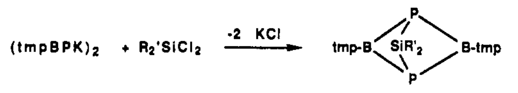

9

(7)

	16	**17**	**18**
R2'Si	Me2Si	Ph2Si	PhMeSi

The new P-monosilylated diphosphadiboretanes **10–14** and the $P_2(BNR_2)_2(SiR'_2)$ cage compounds **15–18** have been characterized by elemental analysis and mass, infrared, and NMR spectroscopy. All of the compounds except **14** display a parent ion in the mass spectra, and fragment ions are consistent with the proposed structures. A measure of the stability of the cage compounds is found in the observation that the most intense ion is the parent ion. The infrared spectra of **10–14** show a weak, but easily identified, band in the region 2281–2226 cm^{-1} that is assigned to the terminal P–H stretch. The position of these bands compares favorably with the range observed for related P-monoborylated diphosphadiboretanes $R_2N\overline{BP(H)B(NR_2)P}B(NR'_2)Cl$[11] and the parent diphosphadiboretanes: **1**, 2267 cm^{-1}; **2**, 2277 cm^{-1}. As expected, a P–H stretching vibration is absent in the cage compounds.

The NMR spectra are summarized in Table X. The $^{11}B\{^1H\}$ NMR spectra for **10–14** show a single resonance in the region δ 47–51, and these values compare favorably with the values for **1**, 47.1, and **2**, 50.8. In each of the compounds containing *i*-Pr_2NB fragments, the ^{11}B resonance appears slightly upfield of the resonance in compounds containing the tmpB fragment. The $^{31}P\{^1H\}$ spectra for **10–14** show two resonances of equal intensity. The lower field resonance is assigned to the diborylphosphane unit, $(R_2NB)_2PH$, since restoration of proton coupling produces a doublet, $^1J_{PH}$ = 179–196 Hz. The higher field resonance is assigned to the diborylsilylphosphane units, $(R_2NB)_2PSiR_3$ or $(R_2NB)_2PSiR_2Cl$, since one-bond P–H coupling is not observed for this fragment. The $^2J_{PP}$ coupling (44–61 Hz) was resolved only for **12** and **13**. The $^{31}P\{^1H\}$ spectra for the cage molecules **15–18** show a single resonance in the range δ 32 to –18. The ^{31}P resonance for **15**, which contains *i*-Pr_2NB units, is significantly upfield of the ^{31}P resonance for the compounds containing the tmpB group. A similar relationship appears when comparing ^{31}P shifts for $P_2(i\text{-}Pr_2NB)_3$, δ –13.0, and $P_2(tmpB)_3$, δ 54.3. The $^{11}B\{^1H\}$ NMR spectra of **15–18** show a single resonance in the range δ 48–52, and once more the resonance for the one molecule containing *i*-Pr_2NB groups appears slightly upfield of the resonance for the molecules containing tmpB groups. The ^1H and $^{13}C\{^1H\}$ NMR spectra are fully consistent with the proposed structures, and the peak assignments are presented in Table X.

The molecular structures of **15** and **17** were examined by single-crystal X-ray diffraction techniques. Views of the molecules are shown in Figures 1 and 2. Selected bond distances and angles are summarized in Table IX. The molecules display a trigonal bipyramidal structure with the three-coordinate phosphorus atoms occupying the apical positions and the R_2NB and Ph_2Si groups residing in the trigonal plane. As a result, these P_2B_2Si cores resemble the P_2B_3 trigonal bipyramidal core structures of $P_2(R_2NB)_3$[10,11] and $P_2(R_2NB)_2(R'_2NB)$.[11] The average P–B bond distances in **15** and **17** are 1.973 and 1.992 Å, respectively. The distances are similar to the average P–B distances in P_2(*i*-Pr_2-

Table X. NMR Data for Compounds **1–28** (23 °C, C_6D_6)

compd	$\delta(^{11}\mathrm{B}\{^{1}\mathrm{H}\})$	$\delta(^{31}\mathrm{P}\{^{1}\mathrm{H}\})^{a}$	$\delta(^{1}\mathrm{H})^{a}$	$\delta(^{13}\mathrm{C}\{^{1}\mathrm{H}\})^{a}$
1	47.1	−162.8	3.9 (PH)	51.6 (CH)
			1.1 (CH$_3$)	23.2 (CH$_3$), 3.5 (CH)
2	50.8	−127.2	4.7 (PH)	58.2 (2), 40.9 (3)
			1.52 (tmp)	30.2 (8), 33.4 (7)
				16.5 (4)
3	50.0	−174.9	4.41 (PH),	70.7 (DME), 59.4 (DME)
		−91.2	4.12 (CH), 3.78 (CH′),	50.6 (CH), 49.3 (CH′)
			3.39 (DME), 3.2 (DME),	24.8 (CH$_3$), 23.5 (CH$_3$′)
			1.45 (CH$_3$), 1.38 (CH$_3$)	
4	53.6	−138.3	5.62 (PH)	71.8 (DME), 58.8 (DME)
		−15.5	3.38, 3.13 (DME)	57.0 (2), 44.5 (3)
			1.93, 1.65 (tmp)	33.3 (7,8), 17.5 (4)
10	48.3	−149.9	0.68 (*Me*$_2$SiPh)	1.7 (*Me*$_2$SiPh)
		−154.0	0.87 (CH$_3$), 4.0 (CH)	21.9 (CH$_3$), 54.8 (CH)
			1.23 (CH$_3$), 3.2 (CH)	24.7 (CH$_3$), 47.4 (CH)
			4.9 (PH)	
			7.1–7.7 (Ph)	127.9–141.0 (Ph)
11	50.6	−107.2	0.85 (Me$_2$Si)	1.1 (Me$_2$Si)
		−130.6	1.4, 1.6 (tmp)	16.5, 33 (br), 42.1, 58.0 (tmp)
			5.9 (PH)	
			7.2–7.9 (Ph)	127.7–141.5 (Ph)
12	47.8	−144.6	0.7 (CH$_3$), 4.0 (CH)	21.4 (CH$_3$), 55.8 (CH)
		−149.7	1.2 (CH$_3$), 3.0 (CH)	24.7 (CH$_3$), 47.2 (CH)
			4.7 (PH)	
			7.1–7.9 (Ph)	128.1–130.3 (Ph)
13	49.0	−106.0	0.9 (SiMe$_2$)	6.3 (SiMe$_2$)
		−123.6	1.2–1.7 (tmp)	16.4, 33.2 (br), 41.8, 58.1 (tm[illegible])
			5.7 (PH)	
14	49.8	−102.6	1.3, 1.5 (tmp)	16.3, 37.0 (br), 41.4, 58.2 (tmp)
		−128.1	5.8 (PH)	
			7.0–8.2 (Ph)	127–138 (Ph)
15	45.4	−18.4	1.1 (CH$_3$), 3.8 (CH)	23.4 (CH$_3$), 52.3 (CH)
			7.1–7.9 (Ph)	127.8–135.7 (Ph)
16	49.2	31.3	0.6 (SiMe$_2$)	2.0 (SiMe$_2$)
			1.49, 1.69, 1.75 (tmp)	15.8, 33.5, 34.6, 40.9, 57.9 (tmp)
17	48.2	32.2	1.45, 1.60, 1.65 (tmp)	15.2, 33.3, 33.8, 37.7, 57.8 (tmp)
			7.1–8.0 (Ph)	127–137 (Ph)
18	48.5	30.6		
19	50.7	−104.5	0.58–0.66 (*Me*$_2$Si–Se*Me*$_2$)	−1.4, −3.4 (*Me*$_2$Si–Si*Me*$_2$)
		−146.6	1.3–1.8 (tmp)	16.5, 34.0 (br), 42.2, 58.1 (tmp)
			5.7 (PH)	
20	57.2	−13.4	0.56 (Me$_2$Si–SiMe$_2$)	−0.22 (Me$_2$Si–SiMe$_2$)
			1.44, 1.46, 1.68, 1.74 (tmp)	16.1, 31.8, 36.7, 42.5, 58.9 (tmp)
21	49.0	−150.6	0.75 (Me$_2$Si–SiMe$_2$)	0.23 (Me$_2$Si–SiMe$_2$)
		−158.0	1.1 (CH$_3$), 4.2 (CH)	22.1 (CH$_3$), 54.9 (CH)
			1.3 (CH$_3$), 3.2 (CH)	24.8 (CH$_3$), 47.1 (CH)
			5.0 (PH)	
23	51.7	−84.9	0.15 (Me$_2$SiSiMe$_2$)	0.03 (Me$_2$SiSiMe$_2$)
			1.14	24.1 (CH$_3$)
			1.24 (CH$_3$), 3.76 (CH)	51.4 (CH)
24	37.7	−39.2	1.12	
		−94.2	1.24 (CH$_3$), 4.9 (CH)	21.2 55.4
			1.26	22.0 (CH$_3$), 46.6 (CH)
			1.35 (CH$_3$), 3.4 (CH)	25.4
			7.3–7.8 (Ph)	127.8–135.7 (Ph)
25	42.1	−27.3	0.64 (SiMe$_2$)	0.14 (SiMe$_2$)
		−42.6	1.5–1.9 (tmp)	14.5, 30.6, 32.5, 35.5–36.6, 58.3 (tmp)
26	42.9	−5.0	1.46, 1.56, 1.58, 1.74 (tmp)	14.3, 32.5, 34.3, 35.4, 58.4 (tmp)
		−35.1	7.3–7.8 (Ph)	127–137 (Ph)
27	54.2	−34.6	0.47, 0.53 (Me$_2$Si–SiMe$_2$)	−0.48, −0.50 (Me$_2$Si–SiMe$_2$)
		−59.4	1.6, 1.7 (tmp)	14.6, 35.1, 38.2, 59.2 (tmp)
28	45.7	−71.9	0.31, 0.53 (Me$_3$Si)	
		−127.8	1.06, 1.17 (CH$_3$), 5.0 (CH)	22.3, 21.3 (CH$_3$), 47.8 (CH)
			1.19, 1.36 (CH$_3$), 3.1 (CH)	27.0, 25.0 (CH$_3$), 54.6 (CH)

[a] Coupling Constants (Hz)

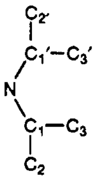

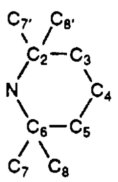

10, $^{3}J_{CP}$ = 5.0 (9), $^{2}J_{CP}$ = 8.2 (*Me*$_2$Si–Ph), $^{3}J_{HH}$ = 6.7 (C_1), $^{3}J_{HH}$ = 6.8 ($C_{1'}$), $^{1}J_{PH}$ = 194, $^{3}J_{PH}$ = 3.4 (*Me*$_2$Si–Ph); **11**, $^{2}J_{CP}$ = 6.7 (*Me*$_2$Si–Ph), $^{3}J_{HP}$ = 2.8 (*Me*$_2$Si–Ph), $^{1}J_{PH}$ = 177, $^{2}J_{PP}$ = 56; **12**, $^{3}J_{CP}$ = 5.0 (C_1), $^{4}J_{CP}$ = 2.3 (C_2), $^{3}J_{HH}$ = 6.7 (C_1), $^{3}J_{HH}$ = 6.8 ($C_{1'}$), $^{1}J_{PH}$ = 200; **13**, $^{2}J_{CP}$ = 3.8 (SiMe$_2$), $^{3}J_{PH}$ = 1.7 (SiMe$_2$), $^{1}J_{PH}$ = 178, $^{2}J_{PP}$ = 44; **14**, $^{3}J_{CP}$ = 3.8 ($C_{7,8}$, tmp), $^{1}J_{PH}$ = 189, $^{2}J_{PP}$ = 56; **15**, $^{3}J_{HH}$ = 6.5; **16**, $^{4}J_{CP}$ = 9.9 ($C_{7,8}$, tmp), $^{4}J_{CP}$ = 6.4 ($C_{7',8'}$); **17**, $^{4}J_{CP}$ = 8.6 ($C_{7,8}$), $^{4}J_{CP}$ = 6.4 ($C_{7',8'}$); **19**, $^{3}J_{CP}$ = 2.7 ($C_{2,6}$), $^{1}J_{PH}$ = 177, $^{2}J_{PP}$ = 44; **20**, $^{2}J_{CP}$ = 5.2 (Me$_2$Si–SiMe$_2$), $^{4}J_{CP}$ = 12.9 ($C_{7,8}$), $^{4}J_{CP}$ = 5.0 ($C_{7',8'}$); **21**, $^{2}J_{CP}$ = 17.1 (Me$_2$Si–SiMe$_2$), $^{3}J_{CP}$ = 5.7 (C_1), $^{4}J_{CP}$ = 1.8 (C_2), $^{3}J_{HH}$ = 5.1 (Me$_2$Si–SiMe$_2$), $^{3}J_{HH}$ = 6.7 (C_1), $^{3}J_{HH}$ = 6.8 ($C_{1'}$), $^{1}J_{PH}$ = 188.6; **23**, $^{2}J_{CP}$ = 5.7, $^{3}J_{HP}$ = 1.9, $^{3}J_{HH}$ = 6.6 (CH), $^{3}J_{HH}$ = 6.8 (CH$_3$), $^{3}J_{HH}$ = 6.7; **24**, $^{3}J_{CP}$ = 5.4 (C_1, i-Pr$_2$N), $^{3}J_{CP}$ = 3.5 ($C_{1'}$), $^{4}J_{CP}$ = 8.2 (C_2), $^{4}J_{CP}$ = 8.7 ($C_{2'}$), $^{3}J_{HH}$ = 6.8 (C_1), $^{3}J_{HH}$ = 6.6 ($C_{1'}$), $^{2}J_{PP}$ = 44.7; **25**, $^{2}J_{CP}$ = 4.6 (SiMe$_2$), $^{3}J_{HP}$ = 2.2 (SiMe$_2$); **26**, $^{2}J_{PP}$ = 29.8; **27**, $^{2}J_{PP}$ = 33.3, $^{3}J_{HP}$ = 4.1 (Me$_2$Si), $^{3}J_{HP}$ = 4.2 (Me$_2$Si); **28**, $^{3}J_{CP}$ = 6.2, $^{3}J_{HH}$ = 6.7, $^{3}J_{HH}$ = 6.6, $^{3}J_{HH}$ = 6.9, $^{3}J_{HH}$ = 6.7, $^{3}J_{HP}$ = 5.9, $^{3}J_{HP}$ = 4.5, $^{2}J_{PP}$ = 33.

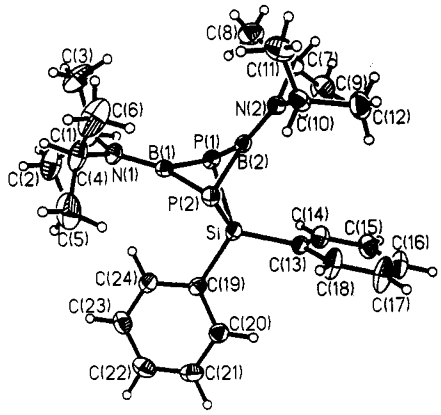

Figure 1. Molecular structure and atom labeling scheme for $P_2(i\text{-}Pr_2NB)_2(SiPh_2)$ (**15**).

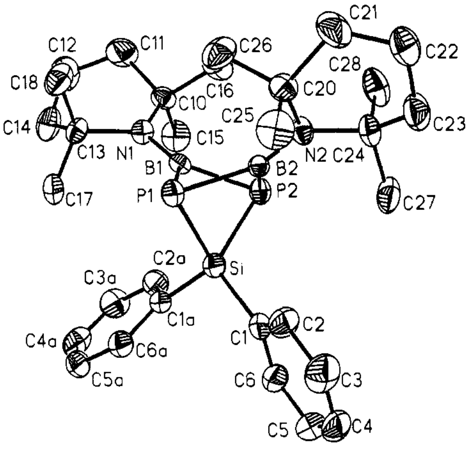

Figure 2. Molecular structure and atom labeling scheme for $P_2(tmpB)_2(SiPh_2)$ (**17**).

$NB)_3$, 1.969 Å, $P_2(i\text{-}Pr_2NB)_2[(Me_3Si)_2NB]$, 1.948 Å, and $P_2(tmpB)_3$, 1.958 Å. The average P–Si bond distances in **15** and **17** are 2.244 and 2.243 Å, respectively, and these are identical to the average P–Si bond distance in $P_4(Me_2Si)_6$, 2.244 Å.[20] The average *exo* B–N bond distances in **15** and **17** are 1.375 and 1.384 Å, respectively. The average $i\text{-}Pr_2N$–B distance in **15** is comparable with the average B–N distance for the $i\text{-}Pr_2N$–B groups in $P_2(i\text{-}Pr_2NB)_2[(Me_3Si)_2NB]$, 1.384 Å, and in $P_2(i\text{-}Pr_2NB)_3$, 1.34(2) Å. The value in **17** is similar to the average B–N distance in $P_2(tmpB)_3$, 1.407 Å.[11]

Since the [1.1.1] bicyclic propellane cage molecules formed easily, it was important to determine if [2.1.1] propellanes could be assembled in this stepwise approach. The 1:1 combination of **4** with $Me_2(Cl)SiSi(Cl)Me_2$ gave the silylated diphosphadiboretane **19**, as described in eq 8. Attempts to isolate this molecule, in analytically pure form failed. However, subsequent treatment of hexane solutions of **19** with *t*-BuLi gave the desired bicycle **20**, as shown in eq 9. Somewhat surprisingly, the 1:1 combination of **3** with $Me_2(Cl)SiSi(Cl)Me_2$ did not produce $i\text{-}Pr_2NBP(H)(i\text{-}Pr_2NB)PSi(Me)_2Si(Cl)Me_2$; however, a small amount (~20%) of bis(diphosphadiboretanyl)disilane **21** formed. This compound is obtained in slightly better yield (~32%) from a 1:2 combination of the reagents, as shown in eq 10. Compound **21** was then treated sequentially with 1 equiv each of *n*-BuLi, $Me_2(Cl)SiSi(Cl)Me_2$, and *t*-BuLi in an attempt to prepare **22**. Instead, the initially sought [2.1.1] bicycle **23** is obtained, together with a very small amount of **3** (eq 11).

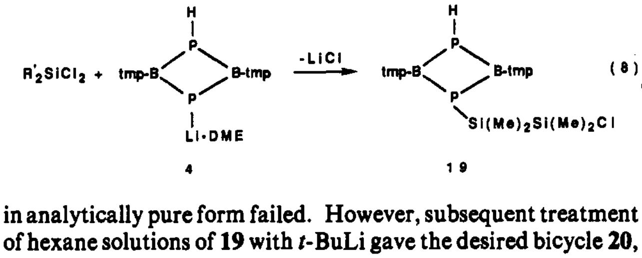

(8)

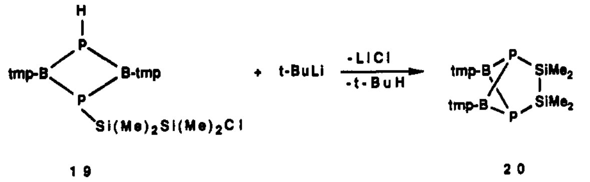

(9)

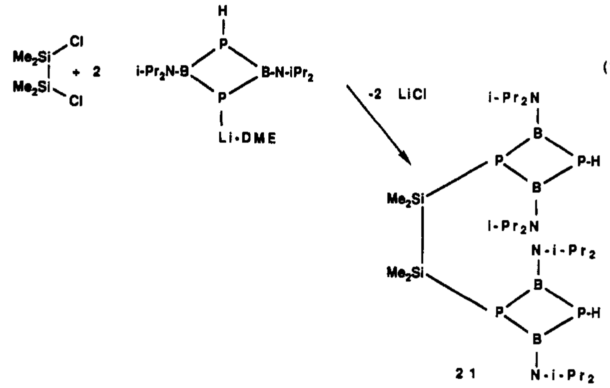

(10)

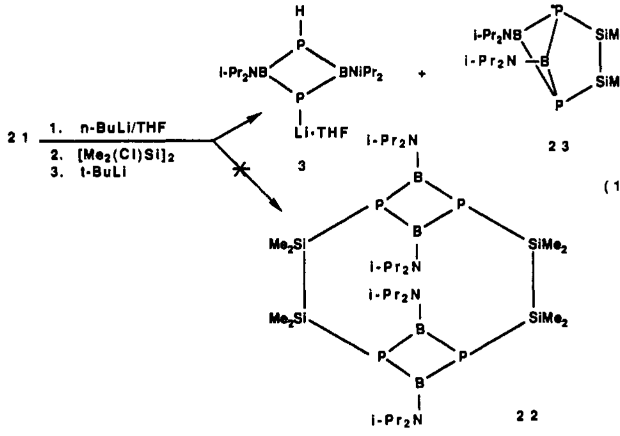

(11)

Compounds **20**, **21**, and **23** were fully characterized by elemental analysis and mass, infrared, and NMR spectroscopy. Compound **19** was only characterized by NMR spectroscopy. The mass spectra of **20** and **23** show strong parent ions, while the parent ion of **21** was not observed. The infrared spectrum of **21**, as expected, shows a medium intensity adsorption at 2261 cm^{-1} that is assigned to ν_{PH}, and a band in this region is absent from **20** and **23**. The $^{11}B\{^1H\}$ NMR spectra for **19** and **20** show single low-field shifts of δ 50.7 and 57.2, respectively, that are assigned to the tmpB fragment. The $^{11}B\{^1H\}$ NMR spectra for **21** and **23** also contain a single resonance, although each is slightly downfield of the usual region found in diphosphadiboretanes. The $^{31}P\{^1H\}$ NMR spectrum for **19**, as expected, shows two equal-intensity doublets centered at δ −104.5 and −146.5 with J_{PP} = 44 Hz. The lower field doublet resonance is further split into a doublet by P–H coupling, $^1J_{PH}$ = 178 Hz. The $^{31}P\{^1H\}$ spectrum of **20** displays a singlet resonance at δ −13.4. The $^{31}P\{^1H\}$ NMR spectrum of **21** displays two doublets centered at δ −150.6 and −158.0, J_{PP} = 49.3 Hz. Restoration of P–H coupling further splits each member of the low-field doublet into a doublet, $^1J_{PH}$ = 189 Hz. The cage molecule **23**, on the other hand, shows a single phosphorus-31 resonance at δ −84.9, with no P–H coupling.

The molecular structures of the new cage molecules **20** and **23** and the bis(diphosphadiboretanyl)disilane precursor **21** were determined by single-crystal X-ray diffraction techniques, and

---

(20) Hönle, W.; Schnering, H. G. v. *Z. Anorg. Allg. Chem.* **1978**, *91*, 442.

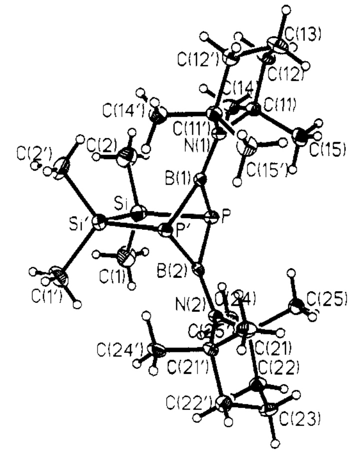

Figure 3. Molecular structure and atom labeling scheme for $P_2(tmpB)_2(Me_2Si)_2$ (**20**).

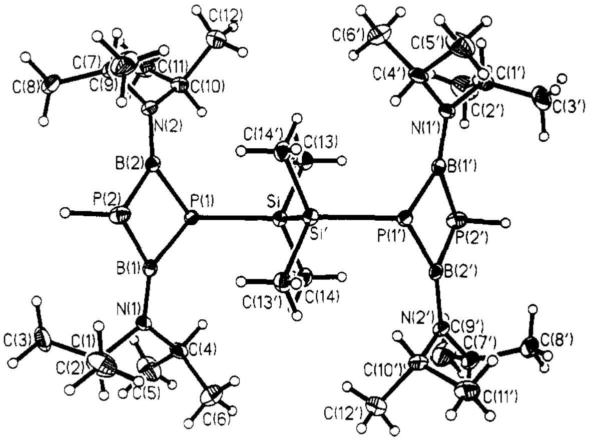

Figure 4. Molecular structure and atom labeling scheme for $[i\text{-}Pr_2NBP(H)B(N\text{-}i\text{-}Pr_2)PSiMe_2]_2$ (**21**).

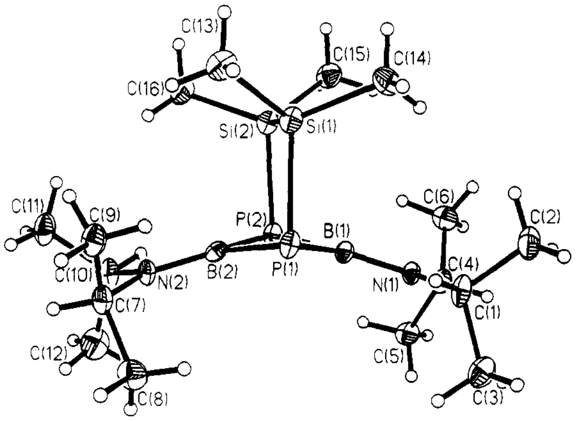

Figure 5. Molecular structure and atom labeling scheme for $P_2(i\text{-}Pr_2NB)_2Si_2Me_4$ (**23**).

views of the molecules are shown in Figures 3–5. Molecule **20** has two perpendicular mirror planes, one that contains B(1), N(1), B(2), and N(2), which bisects the Si–Si′ bond, and one that contains P, P′, Si, and Si′. The bicyclic core structure of **23** is closely related to that of **20**, but the orientation of the *i*-Pr groups reduces the symmetry so that there is only a C_2 axis passing through the Si–Si bond and the center of the B_2P_2 ring. The structure of **21** confirms that two diphosphadiboretane rings are linked through a P–Si–Si′–P′ chain, and there is an inversion center in the molecule located at the midpoint of the Si–Si′ bond. The P–B distances in **20** and **21** are identical, and the average value, 1.978 Å, is closely comparable with the average values in **15** and **17**. On the other hand, the average P–B bond distance, 1.929 Å, in **23** is shorter. The Si–Si bond distances in the cages **20** and **23** are also slightly shorter than the Si–Si distance in the open compound **21**. The P–Si bond distances in **20**, **21**, and **23** are slightly longer than the P–Si distances in the trigonal bipyramidal cage **15**.

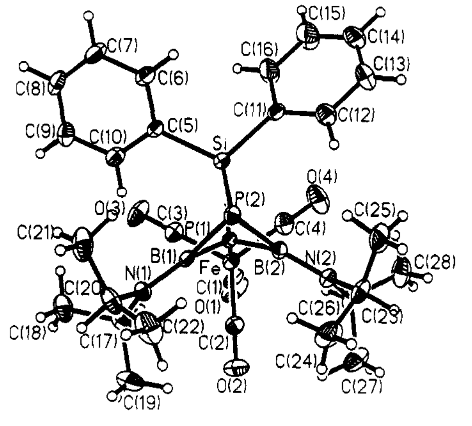

Figure 6. Molecular structure and atom labeling scheme for $P_2(i\text{-}Pr_2NB)_2(SiPh_2)Fe(CO)_4$ (**24**).

Previous studies of the coordination chemistry of the P_2B_3 cage compounds with metal carbonyl fragments $Cr(CO)_5$, $Mo(CO)_5$, and $Fe(CO)_4$[11,21] indicated that only one phosphorus atom would coordinate with a metal fragment. It was therefore interesting to determine if the new cage ligands would form monometallic or bimetallic complexes. Combinations of **15–17**, **20**, and **23** with $Fe_2(CO)_9$ in a 1:1 ratio results in formation of monometallic complexes, as generalized in eq 12. Utilization of excess, $Fe_2(CO)_9$ does not generate bimetallic complexes.

$$Fe_2(CO)_9 + L \xrightarrow{\text{hexane}} Fe(CO)_4L + Fe(CO)_5 \qquad (12)$$

L	15	16	17	20	23
$Fe(CO)_4L$	24	25	26	27	28

Each complex displays a characteristic three-band pattern in the carbonyl region of the infrared spectrum, and the data compare favorably with data for $(i\text{-}Pr_2NB)_3P_2{\cdot}Fe(CO)_4$.[11,21] The $^{11}B\{^1H\}$ NMR spectra for the complexes show a single boron resonance, each shifted 3–8 ppm upfield from the resonance in the corresponding free ligand. The $^{31}P\{^1H\}$ NMR spectra display two resonances. Except for **27**, each peak is shifted significantly upfield from the single resonance of the respective free ligands. In each case, the lower field resonance of the pair is broader, and it is assigned to the metal-coordinated phosphorus atom. Both ^{31}P resonances appear as doublets as a result of P–P coupling that has a magnitude in the range J_{PP} = 24–45 Hz.

The molecular structures of **24** and **25** were determined by single-crystal X-ray diffraction techniques. A view of **24** is shown in Figure 6. There are two independent molecules in the unit cell of **25**, and a view of one of the molecules is shown in Figure 7. The structure determinations confirm that the $Fe(CO)_4$ fragment is bonded to one of the apical phosphorus atoms. The Fe–P distance in **24**, 2.283(1) Å, is slightly longer than the Fe–P distance in $(i\text{-}Pr_2NB)_3P_2{\cdot}Fe(CO)_4$, 2.260(3) Å, and significantly shorter than the Fe–P distance in **25**, 2.328(3) Å (molecule 1) and 2.327(4) Å (molecule 2). All are longer than the Fe–P distance in $Ph_3P{\cdot}Fe(CO)_4$, 2.244(1) Å.[22] The average P–B bond distance 1.972 Å in **24** is identical to that in the free ligand **15**, and the average P–Si bond distance in **24**, 2.257 Å, is comparable to that in **15**. The average B–P–B internal angle about the phosphorus atom, 71.8°, is more open than in the free ligand, 67.3°, while

---

(21) Wood, G. L.; Duesler, E. N.; Paine, R. T.; Nöth, H. *Phosphorus, Sulfur, Silicon* **1989**, *41*, 267.

(22) Riley, P. E.; Davis, R. E. *Inorg. Chem.* **1980**, *18*, 159.

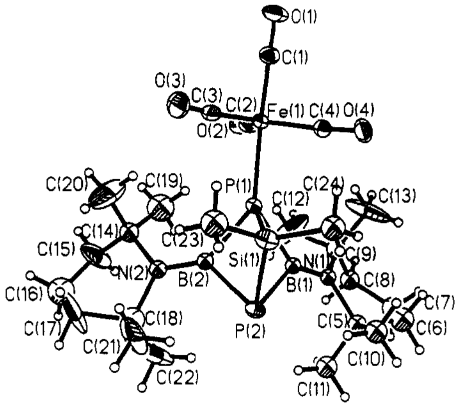

Figure 7. Molecular structure and atom labeling scheme for $P_2(tmpB)_2(SiMe_2)Fe(CO)_4$ (**25**).

the internal angles at the boron atoms are more compressed: **24**, average P–B–P = 95.4°; **15**, 101.2°.

Finally, it is interesting to compare available J_{PP} values, nonbonded P···P distances, and sums of average internal bond angles about apical phosphorus atoms summarized in Table XI. As expected, J_{PP} is detected only in the monometallic complexes where the two phosphorus atoms are magnetically inequivalent. With the few data available, it is not yet possible to make many conclusions; however, the magnitude of J_{PP} (30–45 Hz) is the same for both P_2B_3[11,21] and P_2B_2Si cores. In all cases, the P···P distances are longer in the cage compounds than in the parent diphosphadiboretanes, and the sums of the internal angles about the phosphorus atoms in the cage compounds are much smaller than in the four-membered ring compounds. The P···P nonbonded distances in the P_2B_2Si and $P_2B_2Si_2$ cores are similar or slightly larger than those in the P_2B_3 cores, and the average sum of bond angles at the phosphorus atoms is relatively constant for the five atom cores (212.6–216.8°) except for $P_2(i\text{-}Pr_2NB)_2[(Me_3Si)_2NB]$ (203.6°). The average sum of phosphorus atom angles is much larger for the six atom cores. Where data comparison is possible with **15** and **24**, it is found that coordination of one of the phosphorus atoms leads to reduction in the P···P distance and increase in the sum of internal angles at phosphorus. Thus, the electronic demands of metal coordination appear to "squash down" the cage structure at the cage P atoms, and this is consistent with a high degree of s orbital character in the lone pair donor orbitals.

Table XI. P–P Coupling Constants (Hz), Nonbonded P···P Distances (Å), and Average Sums of Internal Bond Angles (deg) for Selected Compounds

compd	J_{PP}	P···P	$\Sigma\theta(P)_{av}$
$[i\text{-}Pr_2NBPH]_2$		2.862	312.4
$[tmpBPH]_2$		2.735	309.4
$P_2(i\text{-}Pr_2NB)_2[(Me_3Si)_2NB]$		2.980	203.6
$P_2(tmpB)_3$		2.895	214.2
$P_2(i\text{-}Pr_2NB)_2[(Me_3Si)_2NB]Fe(CO)_4$	33		
$P_2(i\text{-}Pr_2NB)_2(tmpB)Cr(CO)_5$	45	2.864	214.4
$P_2(i\text{-}Pr_2NB)(tmpB)_2Fe(CO)_4$	24		
$P_2(i\text{-}Pr_2NB)_2(Ph_2Si)$ (**15**)		3.049	212.6
$P_2(tmpB)_2(Ph_2Si)$ (**17**)		3.026	216.8
$P_2(tmpB)_2(Me_2Si)_2$ (**20**)		2.993	263.9
$P_2(i\text{-}Pr_2NB)_2(Me_2Si)_2$ (**23**)		3.068	256.3
$P_2(i\text{-}Pr_2NB)_2(Ph_2Si)Fe(CO)_4$ (**24**)	45	2.915	225.7
$P_2(tmpB)_2(Me_2Si)Fe(CO)_4$ (**25**)	30	2.862	231.8
$P_2(tmpB)_2(Ph_2Si)Fe(CO)_4$	30		
$P_2(tmpB)_2(Me_2Si)_2Fe(CO)_4$	33		
$P_2(i\text{-}Pr_2NB)_2(Me_2Si)_2Fe(CO)_4$	33		

The systematic, stepwise assembly processes described here for the preparation of P_2B_2Si and $P_2B_2Si_2$ cage compounds suggest that a number of additional $P_xB_yE_z$ cage structures and compositions may be achieved. Continuing efforts to expand this chemistry are underway in our group.

Acknowledgment is made to the National Science Foundation (Grant CHE-8503550) (R.T.P.) and the Fonds der Chemischen Industrie (H.N.) for partial support of this work. Support from the Department of Energy URIP (Grant DE-FG05-86ER-75294) assisted purchase of the JEOL GSX-400 NMR spectrometer, and funds from NSF (Grant CHE-8807358) aided purchase of thhe Bruker WP-250 NMR spectrometer. Selected mass spectral determinations were made at the Midwest Center for Mass Spectrometry with partial support by the NSF Biology Division (Grant DIR 9017262).

Supplementary Material Available: Tables of X-ray data collection parameter, bond distances and angles, anisotropic thermal parameters, and hydrogen atom coordinates (75 pages). Ordering information is given on any current masthead page.